Journal of Volcanology and Geothermal Research 345 (2017) 1–20

Contents lists available at ScienceDirect

Journal of Volcanology and Geothermal Research

journal homepage: www.elsevier.com/locate/jvolgeores

Gravitational slope-deformation of a resurgent caldera: New insights from the mechanical behaviour of Mt. Nuovo tuffs (Ischia Island, Italy)

G.M. Marmoni [a,*], S. Martino [a], M.J. Heap [b], T. Reuschlé [b]

[a] Earth Science Department, Sapienza University of Rome, Piazzale Aldo Moro 5, 00185 Rome, Italy
[b] Géophysique Expérimentale, IPG Strasbourg (CNRS UMR 7516), Strasbourg, France

ARTICLE INFO

Article history:
Received 4 April 2017
Received in revised form 13 July 2017
Accepted 26 July 2017
Available online 31 July 2017

Keywords:
Slope stability
Ischia
Mechanical behaviour
Mass rock creep
Tuff
Hydrothermal system

ABSTRACT

Ischia Island (Italy) is an impressive example of the rare phenomenon of caldera resurgence. The emplacement and replenishment of magmas at shallow depth resulted in a vertical uplift of about 900 m, concentrated in the western portion of Mt. Epomeo (789 m a.s.l.). As a consequence of this uplift, the island has experienced several slope instabilities at different scales since the Holocene, from shallow mass movements to large rock and debris avalanches. These mass wasting events, which mobilised large volumes of greenish alkali-trachytic tuff (the Mt. Epomeo Green Tuff, MEGT), were strictly related to volcano-tectonic activity and the interaction between the volcanic slopes and the hydrothermal system beneath the island. Deep-Seated Gravitational Slope Deformation (DSGSD) at Mt. Nuovo, located adjacent to densely populated coastal villages, is an ongoing process that covers an area of 1.6 km^2. The Mt. Nuovo DSGSD involves a rock mass volume of 190 Mm^3 and is accommodated by a main shear zone and a series of sub-vertical fault zones associated with high-angle joint sets. To improve our understanding of this gravity-induced process, we performed a physical (porosity and permeability) and mechanical (uniaxial and triaxial deformation experiments) characterisation of two ignimbrite deposits - both from the MEGT - that form a significant component of the NW sector of Mt. Epomeo. The main conclusions drawn from our experiments are twofold. First, the presence of water dramatically reduces the strength of the tuffs, suggesting that the movement of fluids within the hydrothermal system could greatly impact slope stability. Second, the transition from brittle (dilatant) to ductile (compactant) behaviour in the tuffs of the MEGT occurs at a very low effective pressure, analogous to a depth of a couple of hundred metres, and that this transition is likely moved closer to the surface in the presence of water. We hypothesise that compactant (porosity decreasing) behaviour at the base of the layer could therefore facilitate slope instability. Although our results show that transient exposure to 300 °C does not influence the short-term strength of the tuff, we speculate that the high in-situ temperature could increase the efficiency of brittle and compactant creep and therefore increase the rate of slope deformation. Taken together, our experimental data highlight a potentially important role for the hydrothermal system (that reaches a minimum depth of ~1 km) in dictating the DSGSD at Mt. Nuovo. An understanding of this deformation process is not only important for the proximal coastal villages, at risk of engulfment by a large debris avalanche, but also for the towns and cities along the coast of the Gulf of Naples that are at risk to a secondary consequence of such an avalanche - a tsunami wave.

1. Introduction

Volcanic resurgence is a common phenomenon in large calderas all over the world and occurs as a direct result of magma inflation or magmatic pressurisation (Smith and Bailey, 1968; Marsh, 1984; Lipman, 1997; Gudmundsson, 1988; Ulusoy et al., 2004; Cole et al., 2005). Magmatic inflation or pressurisation can produce a resurgent block (Civetta et al., 1988; Molin et al., 2003) or cause the caldera floor to dome (e.g., Bailey et al., 1976; Lipman, 1984; Heiken et al., 1990). A strong role is typically ascribed to regional tectonic structures, which can control the tectonic setting of a caldera and influence the shape of the calderic depression as well as its resurgence mechanism (Acocella et al., 2001; Moran-Zenteno et al., 2004; Spinks et al., 2005).

The rejuvenation of calderas can be sufficiently energetic to create reverse faults or reactivate normal faults on the their boundary (Chen et al., 1995; Galindo et al., 2005). Major tectonic elements created during the collapse of the caldera may, in fact, condition the uplift by guiding the resurgence, building new relief characterised by steep slopes (Acocella and Funiciello, 1999) that are prone to the effects of gravity.

* Corresponding author.
E-mail address: gianmarco.marmoni@uniroma1.it (G.M. Marmoni).

http://dx.doi.org/10.1016/j.jvolgeores.2017.07.019
0377-0273/

Tectonic activity can also directly control the triggering of slope instabilities (Radbruch-Hall, 1978) or promote the transition from stationary viscous deformation to accelerating creep (Moro et al., 2007).

Resurgent calderas typically host active geothermal systems (Wohletz and Heiken, 1992; Orsi et al., 1996; Gonzales et al., 2014; Stelling et al., 2016; Molina and Martí, 2016). In these systems, acidic hydrothermal fluids can alter the host rocks, significantly modifying their physical, mechanical, and hydraulic properties (Browne, 1978; del Potro and Hürlimann, 2009; Pola et al., 2012; Frolova et al., 2014; Wyering et al., 2014; Pola et al., 2014; Heap et al., 2015; Sanchez-Alfaro et al., 2016; Heap et al., 2017). Such alteration can therefore weaken the rock mass and promote gravitational instabilities (Lopez and Williams, 1993; Reid et al., 2001; Reid, 2004; John et al., 2008).

Thermal anomalies produced by the presence of long-lived hydrothermal systems can pressurise the system, creating, in the presence of a low-permeability caprock, a fluid overpressure that can also negatively influence rock strength and promote slope instabilities (Day, 1996; Voight and Elsworth, 1997; Reid, 2004). Pore pressure can also rise if the rocks are deformed on a timescale that precludes fluid movement (Heap and Wadsworth, 2016). Further, systematic laboratory tests have demonstrated that temperature can promote thermal stresses leading to thermal microcracking (Fredrich and Wong, 1986; Homand-Etienne and Houpert, 1989; David et al., 1999) and, consequently, increase rock permeability (Vinciguerra et al., 2005; Reuschlé et al., 2006; Nara et al., 2011) that will promote fluid circulation and outgassing. Thermal microcracking can also lead to a decrease in material strength (e.g., Alm et al., 1985). Further, mineral transformations as a result of exposure to high temperature, such as the breakdown of thermally unstable zeolites, the dehydroxylation of clays, or the decarbonation of carbonate minerals, can also induce increases to porosity and permeability and decreases to rock strength (Mollo et al., 2011; Heap et al., 2012, 2013, 2014).

A combination of topographic disequilibrium, due to rapid volcanic growth or resurgence, and passive controls operated by pervasive alteration, inherited discontinuities (i.e. fault, fractures, foliation, depositional surface), and local geothermal anomalies, present a predisposing framework for the triggering of flank instabilities (Clague and Denlinger, 1994; Siebert, 1984; van Wyk de Vries et al., 2000; Romagnoli et al., 2009; Hurlimann and Marti, 2000). Indeed, evidence for large-scale mass movements is provided by symptomatic shallow landforms, the distribution of which is driven and controlled by the interaction of lithological and morpho-structural features (i.e. faults, bedding, foliation) (Dramis and Sorriso-Valvo, 1994; Agliardi et al., 2001; Ambrosi and Crosta, 2006; Esposito et al., 2007; Della Seta et al., 2017), reflecting deep subsurface structural elements. These slope-scale instabilities are commonly defined as deep-seated gravitational slope deformation (DSGSD). The mechanisms driving DSGSD are collectively referred to as mass rock creep (MRC) and are responsible for micro- and meso-scale folding, banding, and shear and tension fractures (Chigira, 1992). Landforms typically produced by MRC include double ridges, composed trenches and bulging (Chigira, 1992; Agliardi et al., 2001).

We focus in this study on the DSGSD affecting Mt. Nuovo, located in the NW sector of Ischia Island, Italy (Fig. 1). The slope in question, described in detail in the next section, results from the asymmetric uplift of Mt. Epomeo (also on Ischia Island), related to the resurgent caldera, for which all the passive controls and conditioning are concurrent and potentially responsible for its onset. We will explore, through laboratory experimentation, the mechanical behaviour and failure modes of two rock types (two porous tuffs) important for the assessment of the stability of the slope. We aim to: i) better understand the mechanisms that drive the slope deformation, ii) verify the consistency of the conceptual model proposed by Della Seta et al. (2015b), and iii) provide the basis for 2D numerical modelling designed to back-analyse the process and estimate the impact of inner forcing, a factor that could initiate slope failure.

2. The Mt. Nuovo (Ischia Island) case study

2.1. Geological and volcanological features

Ischia Island represents the westernmost part of Phlegraean Volcanic District (Central Italy; Fig. 1). The formation of this district is related to the ascent of magma along the Tyrrhenian margin of the Apennine chain during the Plio-Pleistocene extensional phase that generated the Campanian plain graben (Orsi et al., 2003). The Campanian plain graben formed along NW — SE normal fault and conjugated NE — SW transfer faults (Ippolito et al., 1973). Volcanic activity at Ischia Island began prior to 150 ka (Vezzoli, 1988) and continued until the beginning of

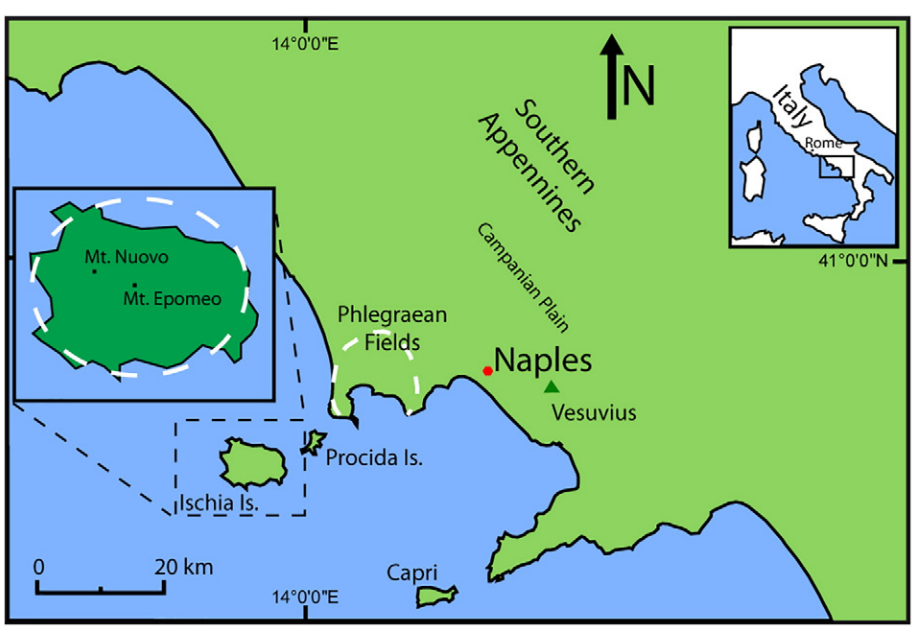

Fig. 1. Location of study area (Ischia Island, Italy) with respect the Campanian Plain. Inset shows a map of Italy. The caldera rims for the Phlegraean Fields and Ischia Island are shown by dashed white lines.

the 14th century (the Arso lava flow in 1302 A.D.). The erupted products belong to the LK-series (low potassium series; Appleton, 1972) and vary in composition (mainly trachytic and alkali-trachytic rocks; Civetta et al., 1991). During a second phase of activity (150 − 74 ka), mostly effusive in style, trachytic and phonolitic lavas were emplaced that largely outcrop as small lava domes on the eastern side of the island (Fig. 2) (Chiesa et al., 1987; de Vita et al., 2006, 2013).

A third period of activity (55 ka) marked the end of a quiescent phase and the age of major explosive caldera-forming eruptions. One of these eruptions led to the emplacement of the Mt. Epomeo Green Tuff (MEGT) (Orsi et al., 1991; Tibaldi and Vezzoli, 1998; Brown et al., 2008), a massive greenish alkali-trachytic pyroclastic flow deposit. The emplacement of the MEGT was originally assumed to be within a seawater-rich environment (Rittmann, 1930), although the signatures of marine emplacement are yet to be fully identified (Altaner et al., 2013). The MEGT, produced by the largest known eruption on Ischia Island, has an estimated volume of 40 km^3 (Tomlinson et al., 2014). Revised proximal-distal tephra correlations define a dispersal axis to the south-southeast and deposits are found as far as 540 km from Ischia Island. Four cm-thick tephra was found in cores from the Ionian Sea and in the mainland at Monticchio Lake (Wulf et al., 2004) and San Gregorio Magno (Tomlinson et al., 2014 and references therein). The MEGT widely outcrops in the central and western sector of Ischia Island and forms the relief of Mt. Epomeo (789 m a.s.l.) and Mt. Nuovo (513 m a.s.l.) (Fig. 1). Brown et al. (2008) divided the MEGT in two components: i) an intra-caldera sequence, made up of two pyroclastic flow deposits (the Upper and Lower MEGT) separated by a volcanoclastic member with a thickness varying from 20 to 50 m; ii) an extra-caldera sequence emplaced outside the caldera rim, characterised by pumice ash-fall deposits and widespread lag-breccia deposits.

According to Vezzoli (1988), the MEGT overlies alkalitrachytic lava flows (133 ky ± 5.5 kyr) that outcrop in Rione Bocca (Fig. 2). This outcrop has been recently interpreted as subvolcanic intrusions with limited lateral continuity (Sbrana and Toccaceli, 2011). The following eruptive period (55 − 33 ka) was punctuated by magmatic and phreatomagmatic explosive eruptions fed by vents located in the NW and SW sector of the island, the deposits of which are exposed in the Citara and Mt. Vico cliffs (Fig. 2) (Rittmann, 1930; Vezzoli, 1988; de Vita et al., 2006). The post-MEGT activity differs in eruptive style and magma composition (Civetta et al., 1991; Brown et al., 2008), showing a progressive increase in magma-water interaction and a different geochemical and isotopic marker (Brown et al., 2014).

The collapse of the caldera was followed by the asymmetric and discontinuous resurgence of the Mt. Epomeo block (Fig. 2). The tectonic setting strongly conditioned the geological evolution of the caldera and its resurgence along NW − SE- (clearly visible in the sharp scarps bordering the Falanga plain), NE − SW-, and N − S-trending faults (Molin et al., 2003), which isolate the polygonal shape of the Ischia resurgent block (Acocella and Funiciello, 1999). The resurgence produced a maximum net uplift of about 900 m in the last 28 − 33 ka, as documented by the current elevation of marine sediments and the temporal clustering of landsliding (Orsi et al., 1991; Buchner et al., 1996; Tibaldi and Vezzoli, 1998; Della Seta et al., 2012). Based on the results of structural surveys and modelling, Acocella and Funiciello (1999) and Molin et al. (2003) proposed a "trapdoor" asymmetric mechanism, tectonically controlled by a network of sub-vertical and NW–SE oriented faults (Fig. 2). According to Molin et al. (2003), the uplift occurred through the reverse reactivation of regional E − W and NE − SW oriented tectonic elements (Fig. 2), and the resultant gravitational outward-sliding of the rock volume bordered by inverse faults. The resurgence resulted in the formation of differentially displaced and tilted polygonal blocks that can be clearly seen in satellite or aerial photos (Fig. 3b). The resurgence could have been generated by the emplacement of a shallow laccolith (Rittmann, 1930; Carlino et al., 2012) or by an increase in volume

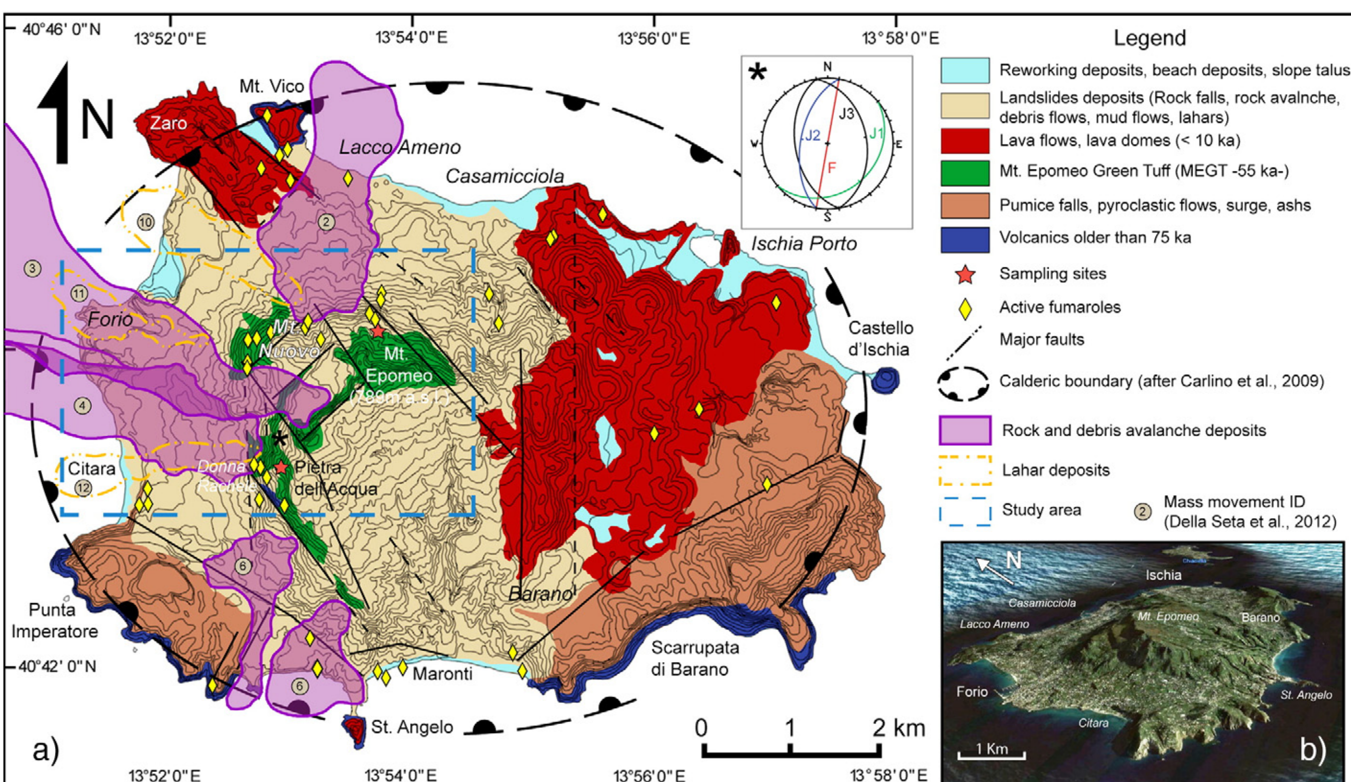

Fig. 2. a) Geological sketch map of Ischia Island. Major mass movements in NW sector are reported here as classified by Della Seta et al. (2012). The study area is indicated by the dashed blue rectangle. b) ENE − WSW satellite photograph of Ischia Island. The asymmetric resurgence is clearly visible. The synthetic stereoplot derive by multiple geomechanical survey across the detachment area of past rock avalanches shows the orientation of the main measured joint sets (location pointed by black asterisk) (Della Seta et al., 2015b). The sampling sites for the blocks of UGT and LGT are indicated by red stars.

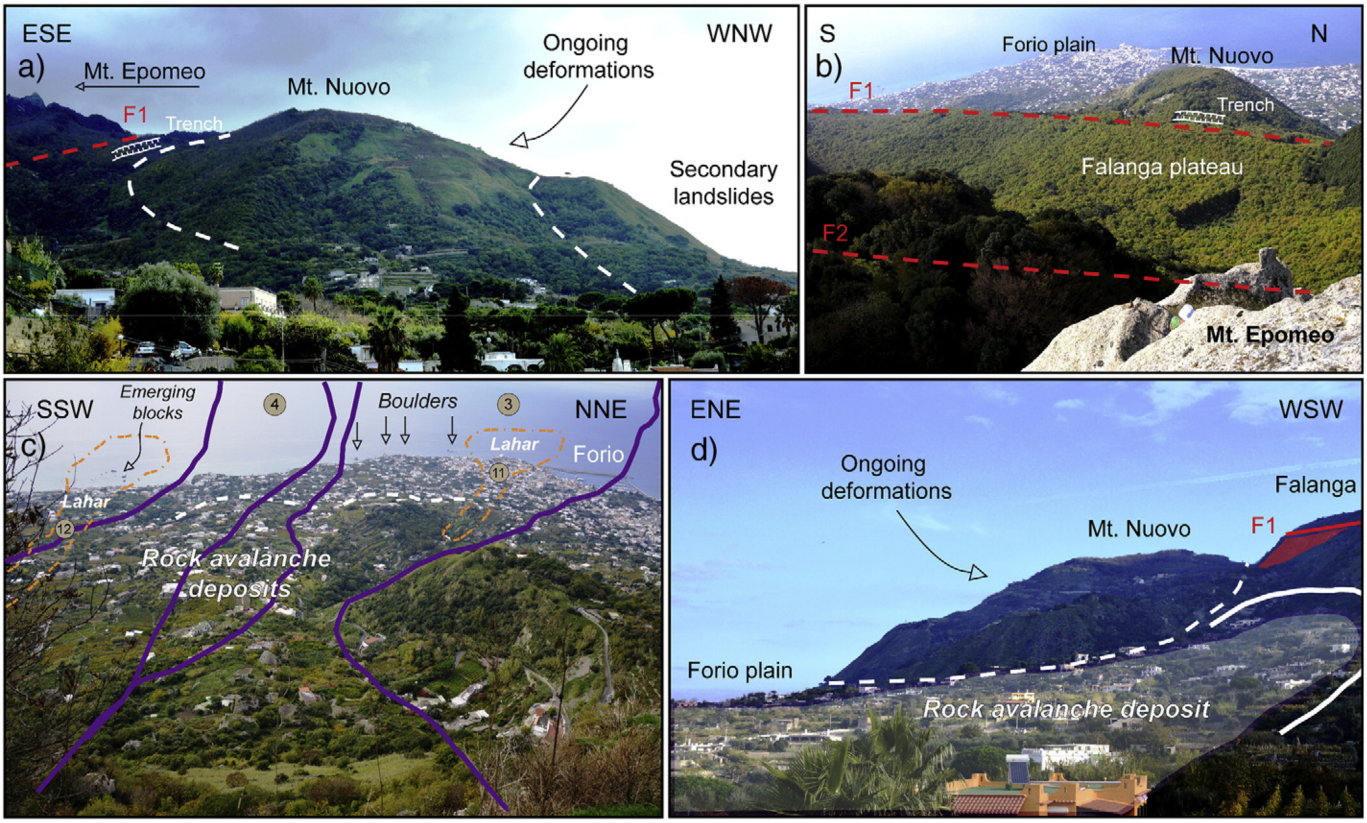

Fig. 3. a) Panoramic view of the Mt. Nuovo area involved in the ongoing gravitational deformation. Schematic traces of gravitational shear zone are shown as white dashed lines. b) View from the top of Mt. Epomeo showing tectonically displaced blocks. Faults that displace the Mt. Nuovo block and Falanga plateau are indicated by F1 and F2, respectively. c) View from the top of the scar area of the rock avalanche deposits (deposit trace delineated by the purple line). Hummocky morphology and linear ridge within the landslide deposits are delineated by a white dashed line. Large blocks and boulders are also indicated. Secondary lahar deposits outcrop in Citara shore and Forio Town (shown in orange). Both the lahars and the avalanche deposit reached the sea. Mass movement ID (grey circles) are shown following the classification proposed by Della Seta et al. (2012). d) Lateral view of the ongoing deformation and apical zone of the rock avalanche deposits.

and pressure in a shallow magmatic chamber (Orsi et al., 1991; Tibaldi and Vezzoli, 1998).

Volcanic activity on the island is documented until 1302 A.D. (the Arso eruption), with small volume events characterised by effusive and sporadic explosive magmatic and hydro-magmatic style eruptions, almost all located in the eastern part of the island (Vezzoli, 1988; Orsi et al., 1996; de Vita et al., 2006, 2010). The present-day state, revealed by differential interferometry synthetic aperture radar (DInSAR) and geodetic measurements, shows a general trend of deflation (ascribed to tectonic- or hydrothermal-related subsidence; Manzo et al., 2006; Sepe et al., 2007) punctuated by landslides.

2.2. The Ischia Island hydrothermal system

The fast resurgence at Ischia Island led to the exhumation of a vigorous hydrothermal system that reaches a minimum depth of ~1 km and is heated by a magmatic reservoir located at a depth of ~2 km (Sbrana et al., 2009; Carlino et al., 2012, 2014). Fluid circulation beneath the island is controlled by the presence of multilayered aquifers hosted in the fractured trachytic lavas (Chiodini et al., 2004) that are recharged by meteoric water and a seawater inlet (Di Napoli et al., 2009, 2011, 2013; Carlino et al., 2014). The hydrothermal system feeds several thermal springs (De Gennaro et al., 1984; Lima et al., 2003) and hot (~100 °C) fumaroles located in the NW sector of the island (the Donna Rachele and Cimmento Rosso fumarolic fields; Fig. 2) (Vezzoli, 1988; Tedesco, 1996; Inguaggiato et al., 2000). The hydrothermal system is characterised by a high heat flux (200 − 400 mW/m^2) and a geothermal gradient ranging between 180 and 220 °C/km (Cataldi et al., 1991; Penta and Conforto, 1951a, 1951b). These high geothermal gradients have attracted interest in geothermal energy exploitation since 1939 to the present day (Carlino et al., 2014; Paoletti et al., 2015).

CO_2 flux measurements provide evidence for a structural control for the outgassing of fluids (Chiodini et al., 2004). The highest fluxes in the Donna Rachele fumarolic field are along NW − SE-trending faults that border Mt. Epomeo block (Fig. 2). The composition of the gases outgassed from the fumaroles located along these faults indicates a high fraction of separated vapour, a testament to the high energy of hydrothermal system at depth (Chiodini et al., 2004). The stress changes responsible for the “explosion” at a well in 1995 (Chiodini et al., 2004 and references therein) provide further evidence for the existence of an energetic system able to produce highly pressurised fluids trapped beneath a low-permeability caprock.

Most of the hydrothermal activity reveals a structural and lithological control for fluid migration to the surface. Gas emissions are typically aligned with the regional tectonic discontinuities (i.e. fault lines) (Chiodini et al., 2004) and concentrate at a particular level in the volcanoclastic stratigraphy - the high-permeability “lithic breccias” layer (Della Seta et al., 2015a, 2015b). The rising fluids migrate laterally along the high-permeability lithic breccias due to the presence of the overlying Lower MEGT unit, which is characterised by a much lower permeability (Della Seta et al., 2015b). Intense alteration can be seen within the lithic breccias at Donna Rachele (Fig. 2) where the fumaroles form as the gas reaches the surface.

2.3. Deep-seated gravitational slope deformation at Mt. Nuovo

The volcano-tectonic activity and, in particular, the resurgence event created a landform prone to slope instabilities. Geological and geomorphological studies (Vezzoli, 1988; Mele and Del Prete, 1998; Del Prete and Mele, 2006; de Vita et al., 2006; Della Seta et al., 2012), combined with archaeological surveys and extensive historical chronicles (Buchner, 1986), document a large number of slope instabilities that differ in size, mechanism, and triggering agent. Excluding shallow landslides that occur in response to intense meteo-climatic events (Ascione et al., 2007; Mazzarella and De Luise, 2007), the island has experienced several large-scale phenomena, including large lahars, debris avalanches, rock avalanches, and slumps in the last 3 ka. In particular, large-scale mass movements (Della Seta et al., 2012) appear to be strictly related to volcano-tectonic processes (de Vita et al., 2006). A new magmatic injection, as hypothesised by de Vita et al. (2006), would result in a reawakening of the resurgence and thus uplift and slope oversteepening, which, accompanied by seismicity (Cubellis, 1985; Alessio et al., 1996), provides the conditions required for slope instabilities. The larger events, which have volumes ranging between 0.5 and 1.5 km^3 ("Ischia Debris Avalanche" (IDA); de Alteriis et al., 2010; "Pietre Rosse Avalanche"; Della Seta et al., 2012) and affected the intensely jointed and hydrothermally altered rock masses of the most uplifted sectors of Mt. Epomeo, were often associated with the intersection of resurgence-related fracture systems and associated fumarolic emissions (Della Seta et al., 2015b).

The most unstable slopes are located to the north, northwest, and southwest of Mt. Epomeo, where large debris avalanches, documented by their huge deposits, have detached from the outer edge of the resurgent block (Fig. 3a − c). In detail, these deposits detached from the hanging wall of NE − SW- and NW − SE-trending faults, which provide the kinematic arrangement for slope deformation (Della Seta et al., 2015b). The temporal occurrence and geometric relation of major mass movements attest to the close connection between volcano-tectonic activity, local seismicity and flank instabilities (Tibaldi and Vezzoli, 1998; de Vita et al., 2006).

The biggest debris avalanches expand into the lowlands south of the town of Forio and into the Serrara Fontana basin, as testified by scar areas and submarine hummocky deposits (Chiocci and de Alteriis, 2006; de Alteriis and Violante, 2009). Part of the proximal facies of these deposits outcrops in Rione Bocca (Fig. 3b), close to the Donna Rachele fumarolic field. The topography of this area consists of typical marginal and distal cliffs, linear ridges, and a distinctive hummocky morphology due to the megaclasts contained within the massive chaotic matrix of MEGT (Siebert, 1984; Glicken, 1998). A large volume of this debris avalanche reached the sea and spread on the continental shelf (Fig. 2c). Tinti et al. (2011) modelled the propagation of the tsunami wave generated by the impact of the IDA, highlighting the severe consequences for the coastal area of the Latium and Campanian regions. The possible earthquake-triggered collapse of the residual portion of Mt. Nuovo was analysed by a simplified limit-equilibrium approach by Paparo and Tinti (2017). This approach reveals a multi-risk scenario from the catastrophic mass failure of Mt. Nuovo (Paparo and Tinti, 2017). The tsunamigenic potential for the potential slope collapse of Mt. Nuovo (Fig. 3) was highlighted by Zaniboni et al. (2013), and was based on the ongoing deep-seated gravitational slope deformation identified by Della Seta et al. (2012) and the recognition of diagnostic features (Crosta et al., 2013 and references therein).

The DSGSD at Mt. Nuovo covers an area of 1.6 km^2 (Fig. 3a and b) and is located to the NW of Mt. Epomeo (i.e. downslope of Falanga plain) in the most uplifted part of the resurgent block (Figs. 2c and 3b). Based on a geological, geomorphological, and geophysical reconstructions, Della Seta et al. (2015b) estimated the volume of rock involved to be 190 Mm^3. These authors also suggested that the DSGSD is accommodated by a low angle, 250 m deep shear zone, leading to a mainly translational mechanism. Such ongoing deformation is clearly seen in the bulging and opening of deep trenches (Fig. 3a and b) that superimposed on and filled by detrital materials, a direct consequence of the tensile stress field acting in this sector. In particular, the Mt. Nuovo DSGSD can be classified as a "type E" structurally-defined compound "constrained at toe" slide (Hungr and Evans, 2004) in which the main rupture surfaces contain high-angle joint sets (related to J2 in the Schmidt net inlayer on Fig. 2).

Based on the reconstructed model, the basal shear zone does not appear to be controlled by any lithological or structural discontinuity, suggesting that different processes must explain its propagation. Geostructural (i.e. faults and joints) and geomorphological similarities (e.g., the geometry of the scar area) between the DSGSD at Mt. Nuovo and adjacent historic debris avalanche (Della Seta et al., 2015b) suggest that ongoing slope deformation involves the residual portion of a wider deforming block that had only partially achieved the conditions for collapse. However, despite the importance of dynamic input in slope stability, given the time-scale and the multiple factors affecting long-term time-dependant gravitational slope deformations, a more comprehensive rheological and thermo-mechanical approach should be considered.

3. Physical and mechanical characterisation

To better understand the mechanism responsible for driving the DSGSD at Mt. Nuovo, as well as to constrain possible factors that can trigger or accelerate the ongoing gravity-induced process, we performed a physical and mechanical characterisation of two pyroclastic units that locally form a significant portion of the slope (Brown et al., 2008; Della Seta et al., 2015b). In particular, our goal was to investigate the mechanical interaction between the hydrothermal system beneath Ischia Island and the development or evolution of slope deformation.

A significant component of this study is a suite of triaxial experiments performed on the two pyroclastic units that form the Mt. Nuovo slope. Although our knowledge of the mechanical behaviour of sedimentary rocks is robust (e.g., Wong and Baud, 2012), only recently have studies begun to investigate the mechanical behaviour of volcanic rocks. Triaxial deformation experiments have been performed on andesite (e.g., Bauer et al., 1981; Smith et al., 2009; Loaiza et al., 2012; Heap et al., 2015; Farquharson et al., 2016; Heap and Wadsworth, 2016; Siratovich et al., 2016; Heap et al., 2017), basalt (e.g., Bauer et al., 1981; Shimada, 1986; Violay et al., 2012; Adelinet et al., 2013; Violay et al., 2015; Zhu et al., 2011), and dacite (e.g., Kennedy et al., 2009; Smith et al., 2011; Kennedy and Russell, 2012; Heap et al., 2016).

However, the recent studies listed above are biased towards extrusive volcanic rocks and studies that investigate the mechanical behaviour and failure mode of tuffs under triaxial conditions are relatively scarce (e.g., Aversa and Evangelista, 1998; Zhu et al., 2011; Heap et al., 2014; Heap et al., 2015). Zhu et al. (2011) performed triaxial experiments on samples of high-porosity (30–40%) tuff from the Alban Hills volcanic complex (Italy). They found that the micromechanism responsible for shear fracturing in the brittle regime was pore-emanating microcracking. In the ductile regime, the cataclastic collapse of pores was the micromechanism driving deformation. Ductility in porous tuffs from Alban Hills was achieved at effective pressures as low as 5 MPa (analogous to a depth of a few hundred metres) (Zhu et al., 2011). The observations of Zhu et al. (2011) are echoed by recent studies on tuff from the Phlegraean Fields (Heap et al., 2014) and Whakaari volcano (New Zealand) (Heap et al., 2015). Both of these latter studies also show that cataclastic pore collapse is the micromechanism responsible for ductile behaviour in high-porosity tuffs. Further, the tuffs of the Phlegraean Fields (Neapolitan Yellow Tuff, porosity 44%, and the grey Campanian Ignimbrite, porosity 48.5%) were ductile at an effective pressure of 5 MPa (Heap et al., 2014), while the tuffs from Whakaari (porosity 30–45%) were ductile between 10 and 20 MPa (Heap et al., 2015). Taken together, these studies suggest that porous tuffs that outcrop at Mt. Nuovo can deform in a ductile manner at shallow depths by the mechanism of cataclastic pore collapse.

3.1. Experimental materials

Intact blocks of rock of both the Upper MEGT (Brown et al., 2008, hereafter named UGT) and the Lower MEGT (hereafter named LGT)

(Fig. 4) were collected from representative outcrops (see Fig. 2 for outcrop location). Textures and mineral assemblages were obtained on representative samples by optical microscopy to recognise the main and accessory minerals and evaluate their modal abundances. In order to identify authigenic phases the samples were also analysed by (1) Scanning Electron Microscope (SEM) using a FEI quanta 400 equipped for microanalysis with an EDAX Genesis system and (2) X-ray diffraction powder (XRPD) analyses using a Siemens D5000 X-ray powder diffractometer, both available at the Earth Science Department of "Sapienza" University of Rome. The XRPD instrument operates in Bragg-Brentano θ/2θ geometry equipped with monochromator (Cu kα 0.154 nm radiation) operating at 60 kV and 300 mA.

The UGT block consists of a pale green-coloured (chartreuse), poorly welded ignimbrite that contains sub-rounded pumice (<2 cm in diameter), lithic fragments (<1 cm in diameter) and crystals within an altered ash matrix. The primary mineral assemblage of the collected UGT block includes fresh sanidine (~16 vol%), plagioclase (~4 vol%), biotite (~4 vol%), clinopyroxene (~1 vol%), and oxide phenocrysts (~1 vol%; Fig. 5a). The phenocrysts occur both as glomerocrysts and as single grains (Fig. 5a). The groundmass consists mainly of glass shards and scarce microlites of alkali-feldspar (in prevalence) and biotite. The glass shards have been partially replaced by zeolites and calcite. Elongated and flattened pores, as well large macropores (0.5 − 1 mm in diameter), are also present within the rock (Fig. 5c and e). SEM and XRPD (Fig. 4c) analyses on these materials reveal the presence of minor quantities of apatite microphenocrysts and authigenic calcite, analcime, K-feldspar, quartz, and sulfides (Fig. 5).

The LGT block shows some petrographic and mineralogical differences with respect to the UGT block. Macroscopically it appears more compact and less vesicular, possibly due to the vesicle sealing as result of the precipitation of secondary minerals. Yellow- to orange-coloured veins/patches reflect the widespread oxidation of the block. The primary mineral assemblage consists of phenocrysts of sanidine (~10 vol%), plagioclase (~2 vol%), biotite (~2 vol%), and oxide (<1 vol%); we did not find any authigenic calcite (Fig. 5b). SEM and XRPD analyses show that argilisation is diffuse, as evidenced by the presence of agglomerations of fibrous minerals (Fig. 5d) and the analcime overgrowths around sanidine phenocrysts (Fig. 5f). The authigenic phases recognised include analcime, K-feldspar, phillipsite, and Fe-sulfides (Fig. 4f and Fig. 5d–f).

On the basis of authigenic mineral associations, Della Seta et al. (2015b) showed that MEGT experienced several low-temperature (<160 °C) alteration events. These events, according to observations by Altaner et al. (2013), are related to the massive debris avalanche that detached from the southern slopes of Mt. Epomeo at Serrara Fontana.

3.2. Experimental methods

All of the laboratory tests were performed at the Géophysique Expérimentale laboratory at the Institut de Physique du Globe de Strasbourg (IPG Strasbourg). Rock physical properties were first measured (connected porosity and permeability) on cylindrical samples of both the UGT and LGT. These samples were cored to a diameter (D) of 20 mm and cut to a nominal length of 40 mm (giving a length to diameter ratio of at least two). We cored the samples from the collected block in the same orientation, and in dry conditions to avoid the washout of the fine fraction. Samples were then precision ground on both sides, to obtain flat and parallel end faces. Based on the size of our experimental samples (D = 20), we avoided large macropores and pumice clasts during our sample preparation.

Prior to measurements of porosity and permeability, the samples were dried in a vacuum oven at 40 °C for at least 24 h. Values of connected porosity and permeability were measured using a helium

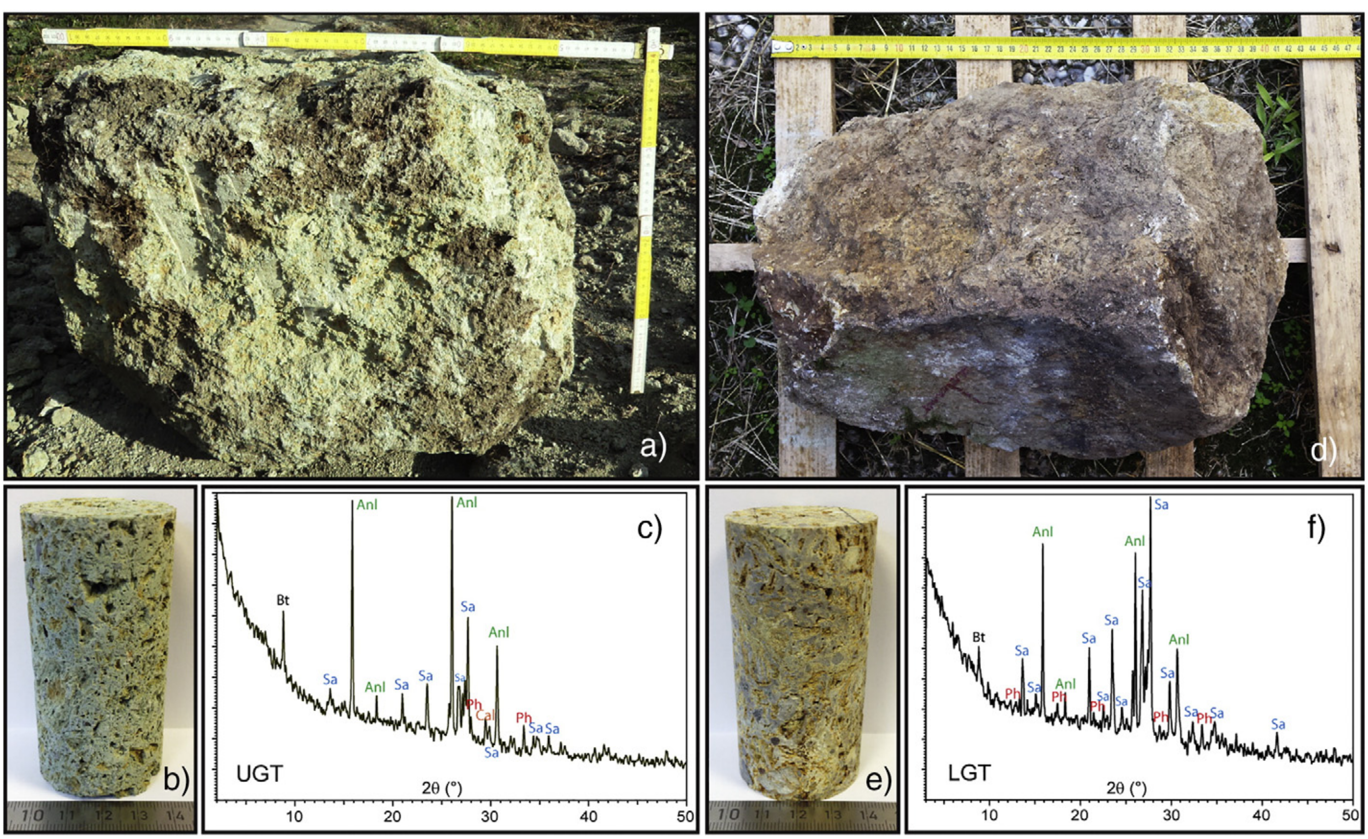

Fig. 4. Photographs of exemplary collected blocks of UGT (a) and LGT (d) and respective laboratory samples (D = 40 mm) (panels b–e). X-ray powder diffraction performed on UGT (c) and LGT (f) reveal the presence of biotite (Bt), sanidine (Sa), analcime (Anl), calcite (Ca), and minor phillipsite (Ph). Based on the diffraction intensity, we assume a higher content of Ph in LGT than in UGT (panels (c) and (f)).

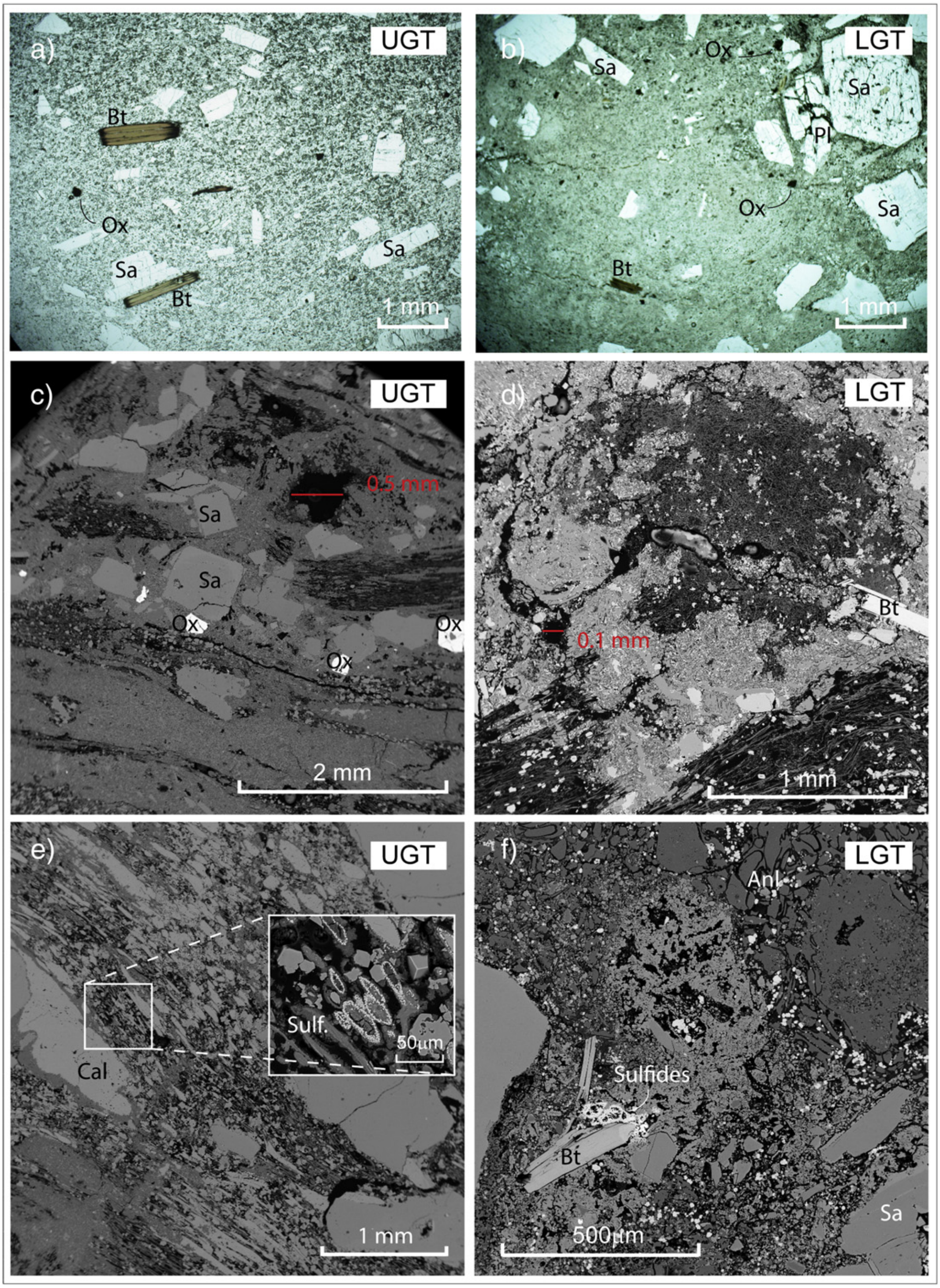

Fig. 5. Optical microscope photomicrographs of the UGT (a) and LGT (b) collected for this study showing the primary mineral assemblage. Sa - sanidine; Bt - biotite; Pl - plagioclase; Ox - oxides. Backscattered scanning electron microscope photomicrographs of features of note showing sulfides in UGT (panel (e)) and LGT (panel (f)). Authigenic calcite is also present (e). Elongated and flattened pores, as well as macropores can be seen in panels (c) and (d). Panels (d) and (f) show alteration textures within the matrix of the LGT (e.g., analcime (Anl) and Fe-sulfides).

pycnometer (AccuPyc II 1340 Micromeritics®) and a steady-state gas (nitrogen) permeameter, respectively (Farquharson et al., 2016; Heap and Kennedy, 2016). Permeability was measured under a confining pressure (P_c) of 1 MPa. Volumetric flow rate Q measurements were taken (using a gas flowmeter) under several pressure gradients ΔP (i.e. the upstream pressure P_u minus the downstream pressure P_d). P_d is simply the atmospheric pressure (taken here to be 101325 Pa). The slope of the graph of Q as a function of ΔP multiplied by the mean pore fluid pressure P_m (i.e. $(P_u + P_d)/2$) yields the raw permeability k_{raw} using the following relation:

$$k_{raw} = \frac{\partial Q}{\partial(\Delta P \cdot P_m)} \frac{(\mu L P_d)}{A}, \tag{1}$$

where μ is the viscosity of the pore fluid (taken as the viscosity of nitrogen at 20 °C = 1.76×10^{-5} Pa s), and L and A are the sample length and cross sectional area of the sample, respectively. We then checked whether any ancillary corrections - namely the Forchheimer and Klinkenberg corrections - were required. We find, due to the high permeability of the materials studied, that the Forchheimer correction was required in each case. The true permeability was therefore taken as the inverse of the y-intercept of the best-fit linear regression in the plot of $1/k_{raw}$ as a function of Q.

Uniaxial compressive strength tests were performed on 20 mm-diameter dry (dried in a vacuum oven at 40 °C for at least 24 h) and water-saturated samples (vacuum-saturated with deionised water and deformed within a water bath) at a constant strain rate of 10^{-5} s^{-1} up to failure. During deformation, axial load and displacement were continuously monitored by the use of a load cell and a linear variable differential transducer (LVDT), respectively. Axial load and displacement were converted to axial stress and strain using the sample dimensions. Larger diameter samples (40 mm in diameter and nominally 80 mm in length) were also prepared in order to investigate any possible scale-effects on both uniaxial compressive strength and deformability of the MEGT.

UCS experiments were also performed on samples (20 mm-diameter) thermally stressed to a range of temperatures up to 300 °C (i.e. temperatures relevant for hydrothermal system at Ischia Island) in order to evaluate the loss of mass through dehydration and any thermally-induced mechanical weakening. The samples to be thermally stressed were selected based on their essentially equal porosity (maximum variation lower than 0.2%) to minimise the influence of sample variability, which could potentially mask any thermal effect. The samples were heated to the target temperature at a rate of 1 °C/min (at room pressure) and left for two hours at the target temperature before being cooled back room temperature at the same rate. We consider that two hours is sufficient based on back-of-the-envelope calculations for the time constant for temperature equilibration, given by r^2/d, where r is the sample radius (1×10^{-2} m) and d is the thermal diffusivity (~1×10^{-6} m^2/s; Hendrickson, 1975). This time constant is about 100 s. We also highlight that one hour at high temperature was sufficient to remove the zeolites present in the Neapolitan Yellow Tuff of the Phlegraean Fields (Heap et al., 2012).

A suite of triaxial tests was performed using a conventional triaxial apparatus (see Heap et al., 2014) on dry and water-saturated samples (20 mm-diameter) at a constant strain rate 10^{-5} s^{-1} under drained conditions (ensured by their high permeability; Table 1; Heap and Wadsworth, 2016). The samples were wrapped in very thin copper jackets to aid their post-deformation recovery from the triaxial apparatus. Experiments were performed under a range of effective pressures (P_{eff}): between 0.5 and 5 MPa for the UGT and between 1 and 10 MPa for the LGT (the testing conditions are reported in Table 1). These pressure conditions (analogous to depth) are relevant for the gravity-driven slope deformation at Mt. Nuovo. For the wet experiments, a pore pressure (P_p) of 10 MPa was chosen. We assume here a simple effective pressure law, $P_{eff} = P_c - \alpha P_p$, were poroelastic constant α is equal to unity. During the hydrostatic phase of the experiment, the confining pressure was increased at a servo-controlled rate of 0.003 MPa s^{-1}. Prior to deformation, the samples were kept at the target effective pressure for at least 12 h to ensure microstructural equilibrium. Due to the inherent variability of porous volcanic rocks, the triaxial tests were performed on samples (D = 20 mm) with mean porosity of 45 ± 2% and 21 ± 1%, for UGT and LGT, respectively (Table 1). Axial load, axial displacement, pore volume change (in the wet experiments), and confining volume change were all monitored during deformation using a load cell, an LVDT, and a pore pressure intensifier/volumometer, respectively. These measurements were converted to axial stress, axial strain, and porosity change, respectively, using the sample dimensions. We use the confining fluid volume change to provide an estimate for the porosity change in the dry experiments. The samples were unloaded slowly following deformation.

Permeability was then remeasured (using the same method as before) on the samples deformed at effective pressures between 0 and 10 MPa under dry conditions to evaluate how the failure mode (i.e. brittle or ductile) might influence fluid migration within the slope. This variation could modify fluid flow in two ways: increasing the ease at which

Table 1
Experimental summary for the experiments performed for this study.

Sample	Connected porosity (%)	Bulk density (kg/m^3)	Intact permeability (m^2)	Test type	Saturation condition (dry/wet)	Thermal stressing temperature (°C)	Confining pressure (MPa)	Pore fluid pressure (MPa)	Effective pressure (MPa)	Peak differential stress (MPa)	Differential stress at C* (MPa)
UGT_2	45.3	1341	2.5×10^{-13}	Triaxial	Wet	room	15	10	5	–	1.45
UGT_6	46	1330	1.4×10^{-13}	Triaxial	Wet	room	12	10	2	–	2.6
UGT_7	45.7	1346	2.4×10^{-13}	Triaxial	Wet	room	11	10	1	–	3.7
UGT_8	48.2	1287	1.0×10^{-13}	Uniaxial	Dry	room	–	–	–	5.3	–
UGT_9	44.4	1376	6.6×10^{-14}	Uniaxial	Wet	room	–	–	–	3.55	–
UGT_10	47	1341	1.9×10^{-13}	Triaxial	Dry	room	1	0	1	6.2	–
UGT_11	48.5	1309	2.5×10^{-13}	Uniaxial	Wet	room	–	–	–	1.8	–
UGT_15	46.4	1360	3.9×10^{-14}	Triaxial	Dry	room	0.5	0	0.5	5.8	–
UGT_20	43.4	1449	–	Hydrostatic	Dry	room	–	–	–	–	11 (P*)
UGT_21	46.1	1381	1.2×10^{-13}	Uniaxial	Dry	100	–	–	–	4.9	–
UGT_22	47	1332	2.2×10^{-13}	Triaxial	Dry	room	5	0	5	–	2.6
UGT_23	46.3	1385	–	Uniaxial	Dry	200	–	–	–	4.9	–
UGT_25	46.4	1374	–	Uniaxial	Dry	300	–	–	–	6.4	–
UGT_26	47	1354	1.0×10^{-13}	Triaxial	Dry	room	2	0	2	4.6	–
UGT_L_2	44.6	1384	–	Uniaxial	Dry	room	–	–	–	4.4	–
LGT_1	20.7	2031	1.1×10^{-16}	Triaxial	Wet	room	11	10	1	27.4	–
LGT_3	20.5	2057	1.5×10^{-16}	Triaxial	Dry	room	5	0	5	40.8	–
LGT_6	21.1	2051	3.2×10^{-16}	Uniaxial	Dry	room	–	–	–	37.8	–
LGT_7	21.7	2022	–	Uniaxial	Dry	200	–	–	–	33.1	–
LGT_9	21.7	2049	1.1×10^{-15}	Uniaxial	Dry	100	–	–	–	26.9	–
LGT_11	20.7	2058	1.3×10^{-16}	Triaxial	Wet	room	15	10	5	–	25.7
LGT_12	21.8	2041	–	Uniaxial	Dry	300	–	–	–	34.5	–
LGT_14	21	2069	–	Uniaxial	Dry	room	–	–	–	33.5	–
LGT_16	20.7	2095	1.9×10^{-16}	Triaxial	Dry	room	1	0	1	39.6	–
LGT_17	20.4	2106	1.4×10^{-16}	Triaxial	Wet	room	12	10	2	34	–
LGT_18	21.4	2076	6.3×10^{-16}	Uniaxial	Wet	room	–	–	–	26	–
LGT_20	20.4	2041	1.1×10^{-16}	Triaxial	Dry	room	2	0	2	35	–
LGT_31	22.7	2057	1.2×10^{-16}	Triaxial	Dry	room	10	0	10	–	41
LGT_L_2	20.2	2039	–	Uniaxial	Dry	room	–	–	–	30	–

fluid can flow (i.e. improving outgassing) along newly formed fractures or decreasing the ease at which fluid can flow, potentially generating fluid overpressures.

We also performed a dry "hydrostatic" experiment ($\sigma_1 = \sigma_2 = \sigma_3$) on a sample of UGT. In this experiment, performed in the triaxial deformation apparatus, the confining pressure was slowly increased while monitoring the sample porosity change (estimated using the change in confining volume). The purpose of this experiment was to define the onset of inelastic compaction as a consequence of hydrostatic pressure, termed P* (see Wong and Baud, 2012). Throughout this study, we adopt the convention that compressive stresses and strains are positive.

4. Results

4.1. Rock physical properties

The average connected porosity of the UGT and the LGT was 47.7 and 21.2%, respectively (Table 1). The average intact permeability of UGT and LGT was 1.6×10^{-13} and 3.0×10^{-16} m^2, respectively (Table 1). The UGT is therefore about a factor of two more porous and about three orders of magnitude more permeable than the LGT (Table 1; Fig. 6). We note that there is no obvious relationship between porosity and permeability within the UGT and LGT sample sets (Fig. 6).

4.2. Uniaxial compression experiments

Wet and dry UCS tests were performed on both rock types (UGT and LGT). These data, together with the UCS values derived for large-diameter samples and ones obtained following thermal stressing, are plotted as a function of connected porosity in Fig. 6b. We find that the LGT (UCS values between ~25 and ~38 MPa; Table 1) is much stronger than the UGT (UCS values between ~2 and ~7 MPa; Table 1). The UCS tests performed on larger-diameter samples (i.e. UGT_L2 and LGT_L2; Table 1) show comparable results, with maximum strength of 4.4 and 30 MPa, respectively (Fig. 7). In detail, our data show that dry UCS is systematically higher than wet UCS, an observation that holds true for both UGT (Fig. 7a) and LGT (Fig. 7b). The ratio between wet and dry UCS, expressed as a percentage, is 35 and 68% for UGT and LGT, respectively. However, we find that there is no systematic change in UCS for the samples thermally stressed to 100, 200, and 300 °C (Fig. 8c and d).

4.3. Triaxial compression experiments

To inform on the deformation mechanism driving the ongoing deep slope deformation, a suite of triaxial deformation experiments was performed on dry and wet samples of UGT and LGT to better understand the role of confining pressure on the mechanical behaviour and failure mode of the MEGT. These data, that can be considered representative of the sample lengthscale, will represent the fundamental data for mechanical zoning of rock masses which, following equivalent continuum approaches (Hoek et al., 2002; Sitharam et al., 2001), will allow laboratory results to be upscaled to longer lengthscales (e.g., the slope scale) by accounting for slope scale discontinuities, such as joint sets (Esposito et al., 2007).

The mechanical data for the dry experiments are shown in Fig. 8. The stress-strain curves for the dry samples of UGT are typical of those for rock deformed in compression (e.g., Hoek and Bieniawski, 1965). They all contain an initial concave part (typically attributed to the closure of pre-existing microcracks) followed by a pseudo-linear elastic portion (Fig. 8a). A convex stage, associated which irreversible deformation, occurs before a peak stress is reached (Fig. 8a). A strain-softening phase (i.e. a stress drop, the mechanical signature of brittle deformation) follows the peak stress (Fig. 8a). Despite the observation of strain-softening, the experiments performed at effective pressures of 1, 2, and 5 MPa were compactant throughout, as shown in the porosity change data (red curves in Fig. 8a); only the experiment at an effective pressure of 0.5 MPa was dilatant (blue curve in Fig. 8a).

The stress-strain curves for the dry LGT samples are qualitatively similar to those of the UGT (Fig. 8b). However, the amount of strain softening following the peak stress is gradually reduced as effective pressure is increased and, at an effective pressure of 10 MPa, there is no strain softening mechanical behaviour indicative of a ductile response. This assertion is supported by the porosity change data (Fig. 8b) that show that dry LGT was dilatant at effective pressures between 1 and 5 MPa and was compactant at an effective pressure of 10 MPa.

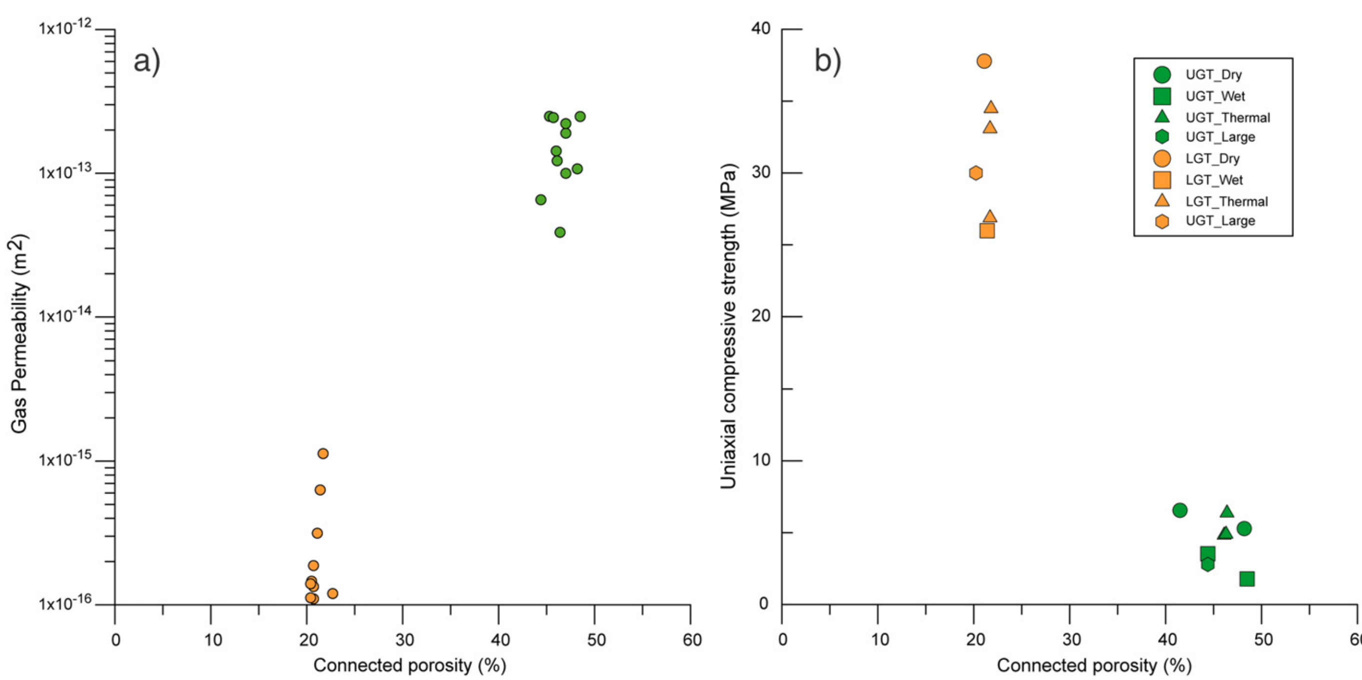

Fig. 6. a) Intact gas permeability as a function of connected porosity for the UGT (green symbols) and the LGT (orange symbols). Measurements were performed under a confining pressure of 1 MPa. b) Uniaxial compressive strength (UCS) as a function of connected porosity for dry, wet, and thermally stressed samples of UGT (green symbols) and LGT (orange symbols).

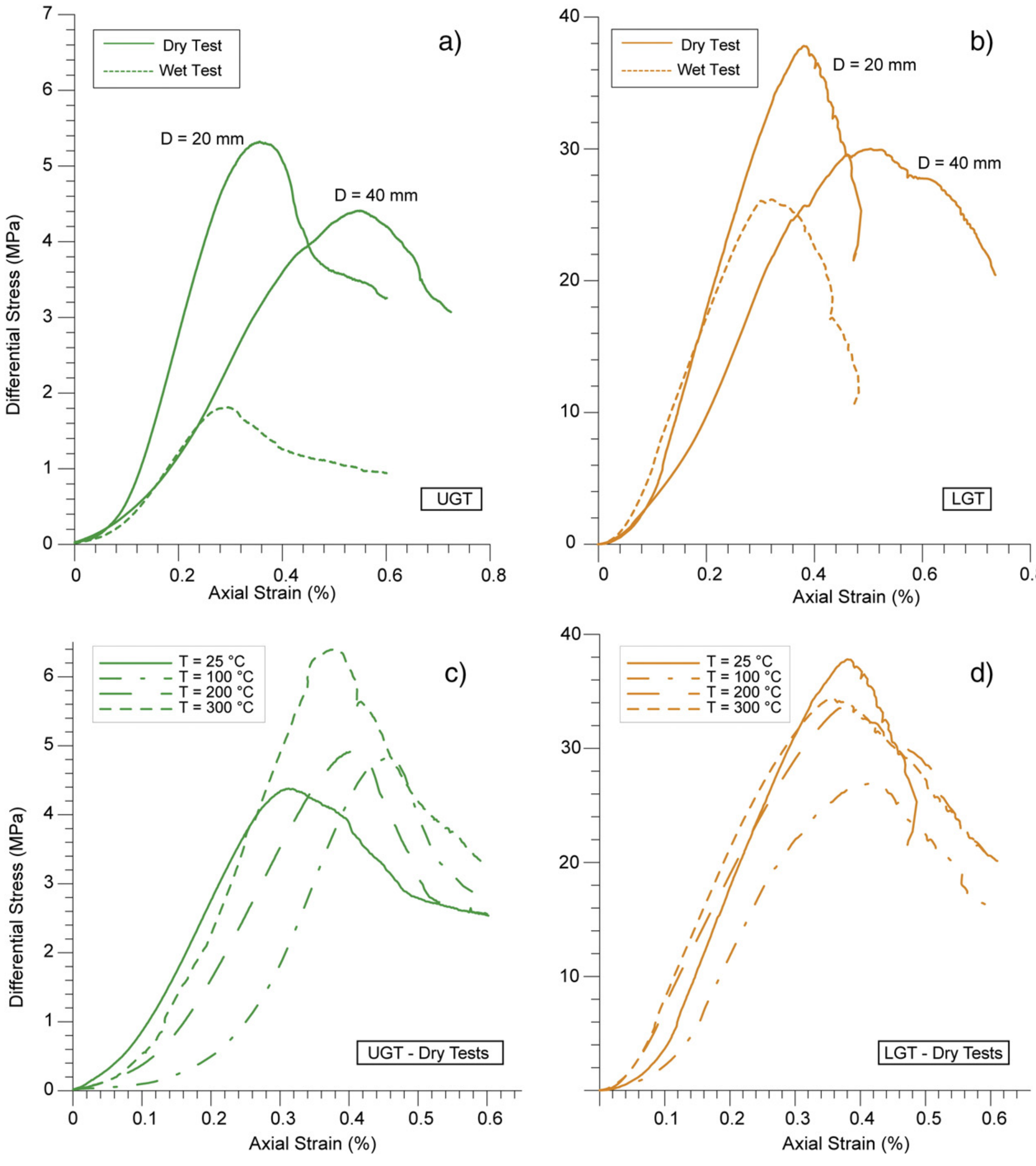

Fig. 7. Stress-strain curves from uniaxial compressive strength (UCS) tests on UGT and LGT. Panels (a) and (b) show dry (solid curves) and wet (dashed curves) experiments performed on samples of UGT and LGT, respectively. Stress-strain curves for the larger diameter samples (D = 40 mm) show that their strength are not dissimilar to those found when using the smaller diameter (D = 20 mm) samples. Panels (c) and (d) show stress-strain curves for thermally stressed (from 100 to 300 °C) samples of UGT and LGT, respectively, together with curves for intact UGT and LGT samples. All experiments were performed at room temperature.

If we interpret the compactant UGT experiments as ductile, the brittle to ductile transition for dry UGT occurs at an effective pressure of about 1 MPa (equivalent to a depth of ~100–200 m). By contrast, the brittle to ductile transition in dry LGT occurs at an effective pressure between 5 and 10 MPa (depth up to ~1 km).

The mechanical data for the wet (pore pressure = 10 MPa) experiments on samples of UGT and LGT are shown in Fig. 9. The presence of water influenced the mechanical behaviour in two ways. First, the peak stress at an equivalent effective pressure is lower when wet than in the dry condition (Figs. 9 and 10). Second, although the wet and dry experiments performed on LGT at an effective pressure of 5 MPa were both dilatant (i.e. brittle) (Fig. 8b), the experiment performed in the wet condition showed much less in terms of dilation (Fig. 9b). Indeed, at the end of the wet experiment performed at 5 MPa, the sample had suffered net compaction (Fig. 9b).

4.4. Post-deformation permeability measurements

In order to understand how failure modes (i.e. brittle or ductile) can influence permeability and thus condition fluid migration in the shallow part of the slope, gas permeability measurements were performed under a confining pressure of 1 MPa on samples of dry UGT and LGT deformed by triaxial tests. These data are plotted alongside the intact permeability values as a function of the effective pressure during deformation in Fig.

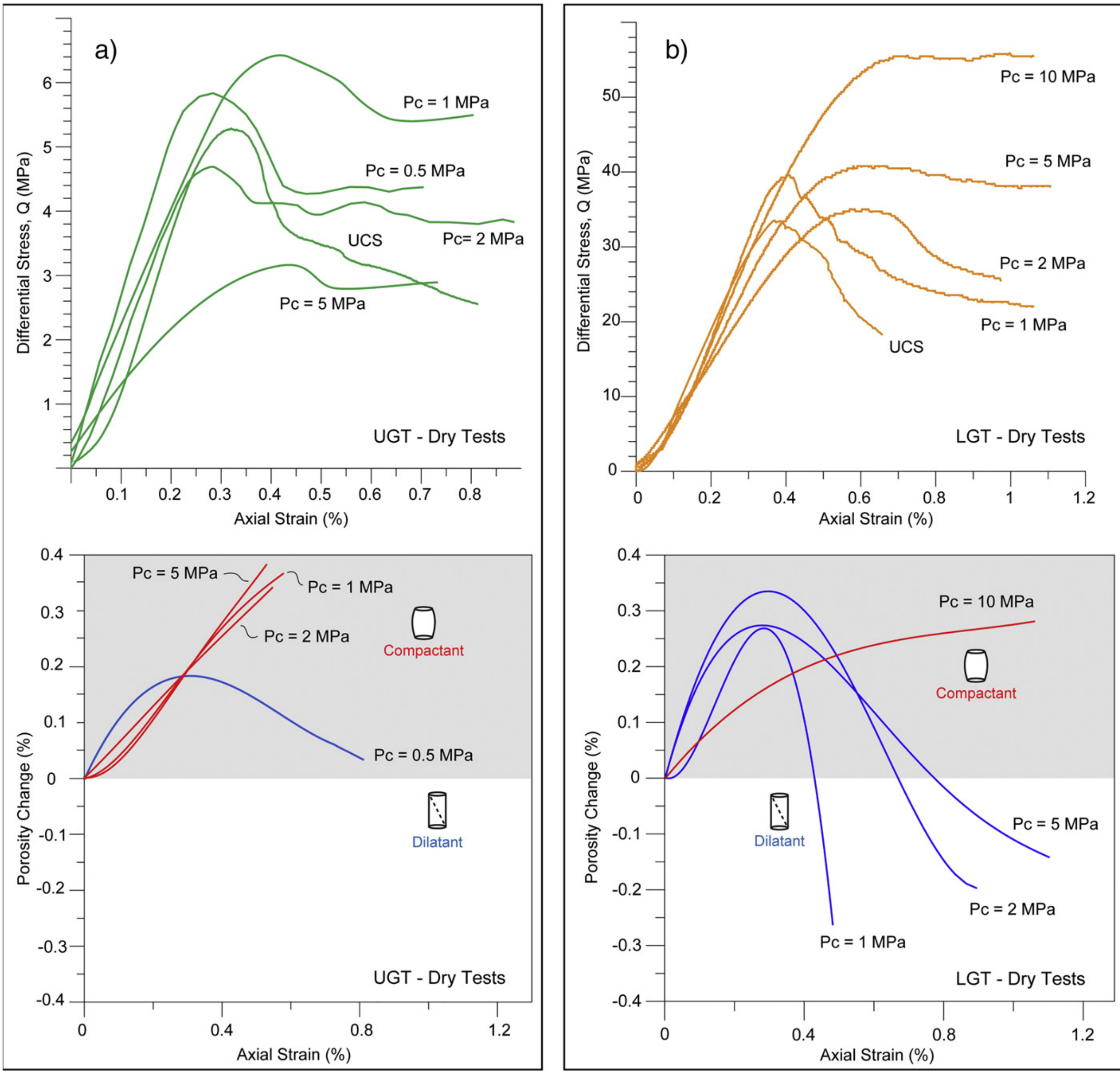

Fig. 8. Dry triaxial tests on UGT (a) and LGT (b). The effective pressure of the experiment is labelled next to each curve. The porosity change was estimated using the change in confining fluid volume. Dilatant porosity change curves are shown in blue and compactant porosity change curves are shown in red. The grey and white zones highlight net compaction and net dilation in the porosity change graphs, respectively.

10. For UGT we find that permeability increased (by a factor between two and four) following deformation at effective pressures between 0 and 2 MPa, and that permeability was decreased by a factor of about two following deformation at 5 MPa (Fig. 10). The permeability of LGT increased by up to two orders of magnitude following deformation at effective pressures between 0 and 5 MPa (Fig. 10). Following deformation at an effective pressure of 10 MPa, the permeability of the LGT only showed a very minor increase from the intact permeability (Fig. 10).

5. Discussion

5.1. Rock physical properties

The lower porosity, and therefore lower permeability, of the LGT compared to the UGT is the result of hydrothermal alteration experienced by the LGT (Fig. 5). The intact permeability of the UGT and LGT - 6×10^{-13} and 3.0×10^{-16} m^2, respectively - could be considered as low when one considers their high porosity (47.7 and 21.2%, respectively). These results align with previously published measurements for high porosity tuff (Montanaro et al., 2016). The lower porosity of LGT, combined with clay-alteration of rock matrix (Fig. 5), hinders fluid flow and, as such, the LGT layer could therefore be considered a fluid barrier (i.e. aquitard). The hydrothermal alteration filled the porous structure, densifying the deposit and thus lowering its permeability. As an example, the permeability of the uniformly sorted Fontainebleau sandstone containing a porosity of ~21% (i.e. the same porosity as LGT) is ~2.5×10^{-12} m^2 (Bourbié and Zinszner, 1985). It has been previously observed that high-porosity tuffs are characterised by anonymously low permeabilities, thought to be a consequence of their complex porosity structure

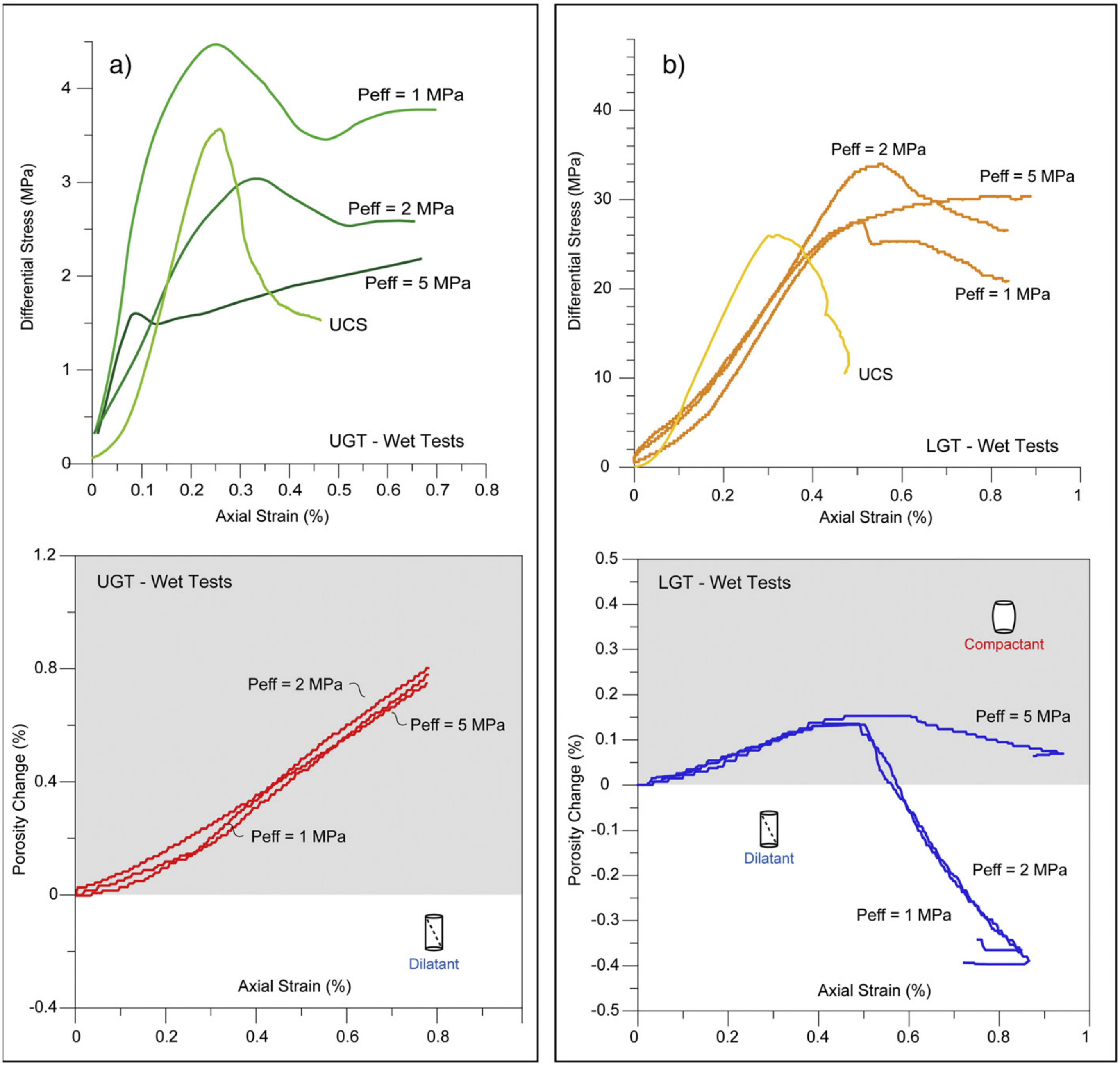

Fig. 9. Wet triaxial tests on UGT (a) and LGT (b). The effective pressure of the experiment is labelled next to each curve. The pore pressure for all experiments was 10 MPa. Dilatant porosity change curves are shown in blue and compactant porosity change curves are shown in red. The grey and white zones highlight net compaction and net dilation in the porosity change graphs, respectively.

(Vinciguerra et al., 2009; Heap et al., 2014). For example, the Neapolitan Yellow Tuff (from the Phlegraean Fields), which contains a porosity of ~44%, has a permeability of ~10^{-15} s^{-1} (Heap et al., 2014). The absence of a correlation between the porosity and permeability of samples within the lithological groups (i.e. UGT and LGT) is likely the result of the natural variability between samples cored from the same block of material. At longer lengthscales, meso- and macro-scale fractures can govern the fluid mobility and thus the rock mass permeability (e.g., Matsuki et al., 2006; Heap and Kennedy, 2016). With this in mind, an upscaling approach could be applied that relates intact laboratory permeability measurements and in-situ hydraulic conductivity measurements by means of rock mass quality indexes (El-Naqa, 2001; Barton, 2002). This approach can therefore upscale measurements to be used in the hydro-mechanical numerical model of the slope system.

Finally, we note that the porosities of our samples differ from the “slightly altered” and “highly altered” samples of Green Tuff reported by Pola et al. (2014), which were 25.5 and 29.7%, respectively, a testament to the variable nature of the MEGT.

5.2. Uniaxial compression experiments

Our data show that the LGT has a higher UCS than the UGT (Fig. 6b), interpreted a consequence of its lower porosity as a result of intense hydrothermal alteration (Fig. 5). Previous experimental studies on volcanic rocks have shown that porosity is negatively correlated with UCS (e.g., Al-Harthi et al., 1999; Schaefer et al., 2015). Our values of UCS (Fig. 6b) are within the range found for the “slightly altered” and “highly altered” samples of Green Tuff by Pola et al. (2014), which were 5.7 ± 0.9 (25.5% porosity) and 16.3 ± 0.9 (29.7% porosity), respectively. UCS

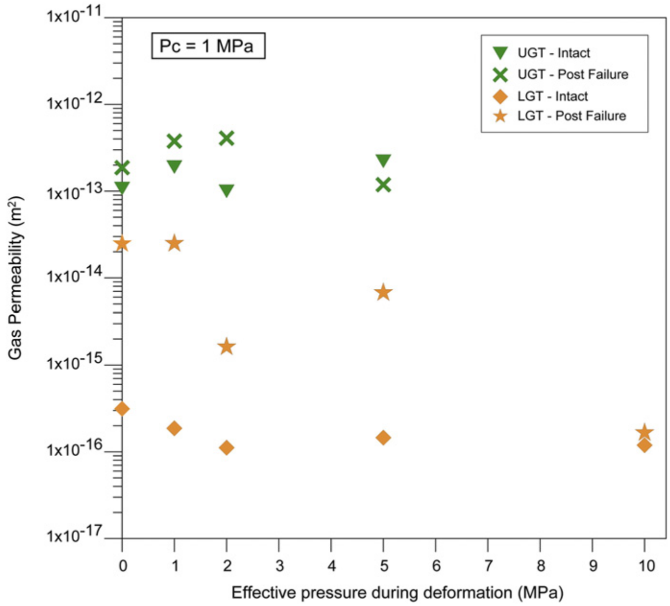

Fig. 10. The change in gas permeability following deformation at effective pressures between 0 and 10 MPa for samples of dry UGT and LGT. Measurements were performed under a confining pressure (Pc) of 1 MPa.

tests on larger diameter (40 mm) samples show a comparable strength respect to the small diameter (D = 20 mm) samples (Figs. 6b and 7a–b). We further note the strengths of the 20 and 40 mm-diameter samples are almost identical if the values are corrected to equivalent 50 mm diameter strength using the empirical relationship from Hoek and Brown (1980):

$$\sigma_{cd} = \sigma_{50}\left(\frac{50}{D}\right)^{0.18} \tag{2}$$

where σ_{cd} is the strength measured on a sample with diameter, D, and σ_{50} is the equivalent strength of a sample with a diameter of 50 mm. Due to size limitations of the triaxial test apparatus, a scale-effect on the mechanical behaviour could not be investigated at higher confining pressures.

The mechanical properties and its response to applied stressed is strongly controlled by the presence of water, as previously observed in other tuffs (Heard et al., 1973; Schultz and Li, 1995; Topal and Doyuran, 1997; Topal and Sözmen, 2003; Tuncay, 2009; Zhu et al., 2011), as well as in sandstones (e.g., Hawkins and McConnell, 1992; Baud et al., 2000; Demarco et al., 2007) and limestones (e.g., Vásárhelyi and Ván, 2006; Baud et al., 2009). Altered or weathered volcanic rocks by their nature are highly sensitive to moisture content variation, which can be stored within the structure of clay minerals (Deriszadeh and Wong, 2014). This effect becomes important where fluids can efficiently circulate and interact with the rock mass and where cyclic (seasonal or aperiodic) perturbations occur (Vergara and Triantafyllidis, 2015). The rocks within a hydrothermal system are therefore likely to be particularly prone to water-weakening. Indeed, experiments on sandstone have previously shown that the UCS_{wet}/UCS_{dry} ratio is higher for clay-rich sandstones than for siliceous sandstones (e.g., Hawkins and McConnell, 1992). Our data show that the UCS of both UGT and LGT is lower in the presence of water. We plot our UCS_{wet}/UCS_{dry} ratios for UGT and LGT — 34% and 69%, respectively, together with previously published data on water-weakening in tuffs (compiled in Zhu et al., 2011), in Fig. 11. When compared with the previously published data on porous tuffs (Montanaro et al., 2016; Marmoni et al., 2017 and references therein), the UGT and LGT show a high level of water-weakening (Fig. 11). This is attributed here to the documented presence of zeolite (analcime and minor phillipsite) (Fig. 4) within UGT and LGT (Fig. 5). Although not detected in our SEM or XRPD analysis, the presence of chabazite and illite/smectite was documented by Altaner et al. (2013) and Pola et al. (2012), testifying once again to the variability of the alteration within the MEGT.

Our uniaxial data also show that transient exposure to 100, 200, and 300 °C (the temperatures expected within the shallow part of the slope at Mt. Nuovo) does not systematically influence the short-term strength of UGT or LGT (Fig. 8c and d). However, a previous study showed a significant and systematic reduction in strength for thermally stressed zeolite-bearing tuff (Heap et al., 2012). These authors found that zeolites contained within the rock dehydrated and broke-down at temperatures of a couple of hundred degrees. Since zeolites such as chabazite and phillipsite represent the "cement" that promoted the initial lithification of the original pozzolanic material, their breakdown significantly reduced the strength of the tuff (Heap et al., 2012). Although it is therefore surprising that we do not observe a weakening with thermal stressing temperature in UGT and LGT, we must conclude that any influence is likely masked by the natural variability of samples cored from the same block of material (even when samples were selected for their similarity in porosity), or could be explained by the low content of zeolites within the tested materials (Fig. 4).

5.3. Triaxial compression experiments

Our triaxial experiments show that the UGT shows compactant behaviour at effective stresses of ~1 MPa (Figs. 9 and 10), corresponding to a depth between ~100–200 m. The onset of compactant (i.e. ductile) behaviour occurs at a higher effective pressure of ~10 MPa for LGT (Figs. 9 and 10), a consequence of its lower porosity (a result of intense hydrothermal alteration; Fig. 5). Rocks containing higher porosities typically transition to ductile behaviour at lower effective pressures (e.g., Wong and Baud, 2012; Heap et al., 2015). As noted above, high-porosity tuffs (30–50%) have previously been shown to switch to compactant (i.e. ductile) behaviour at very low effective pressures, equivalent to depths of a few hundred metres (e.g., Zhu et al., 2011; Heap et al., 2014, 2015). We infer here that the mechanism driving ductile behaviour in the tuffs studied herein is cataclastic pore collapse, as observed in previous

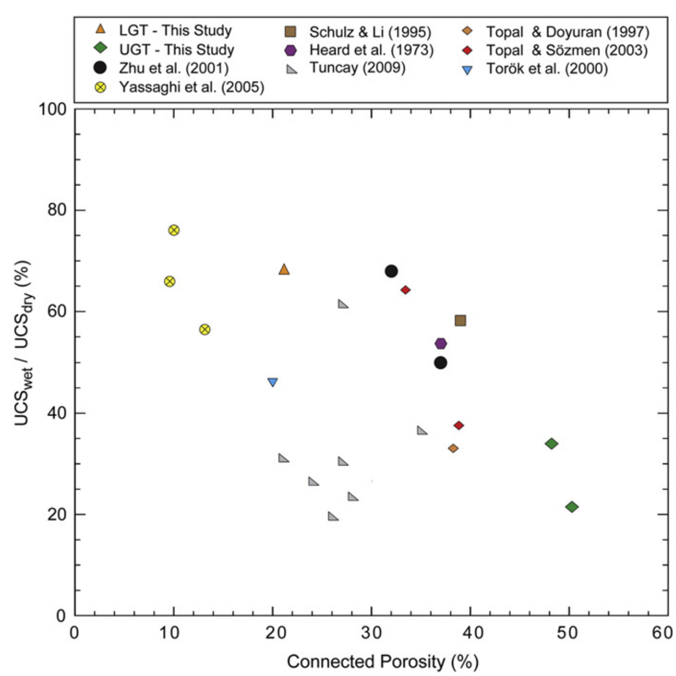

Fig. 11. The ratio of UCS_{wet}/UCS_{dry}, expressed as a percentage, for UGT and LGT and a compilation of previously published data on water-weakening in tuffs. Modified after Zhu et al. (2011).

experimental studies on high-porosity tuffs (e.g., Zhu et al., 2011; Heap et al., 2014, 2015).

The triaxial data for UGT (the rock type for which we have the most data) can be summarised on a graph of differential stress (Q; i.e. σ_1–σ_3) required for failure versus effective mean stress (P, where $P = (\sigma_1 + 2\sigma_3)/3 - P_p$) (Fig. 12). The peak stress delineates the failure envelope in the brittle regime, while the onset of shear-enhanced compaction, termed C*, maps out the compactive yield envelope. Graphs of this type map the stress conditions for which the rock is intact (inside the failure envelope) and the stress conditions for which the rock will fail in the brittle regime (outside the failure envelope on the left-hand side) and the ductile regime (outside the failure envelope on the right-hand side). The onset of hydrostatic pore collapse, termed P*, plots along the *x*-axis (since Q = 0 MPa). Although the data are few, we could conclude that the compactive yield envelope for UGT is linear, as observed for recent studies on compaction in volcanic rocks (Heap et al., 2015, 2015, 2016). By contrast, compactive yield envelopes for porous sedimentary rocks are typically parabolic (reviewed in Wong and Baud, 2012). A linear compactive yield envelope has been previously interpreted as the consequence of pre-existing microcracks and, although we could arrive at the same conclusion for the UGT (microcracks are present in the intact material; Fig. 5), we highlight the extreme microstructural complexity of this material. More data on these tuffs, and other porous volcanic materials, are required to better understand the rock attributes that produce linear compactive yield envelopes.

The construction of the failure envelope for UGT allows us to compare its behaviour to other porous tuffs. The data of this study (average porosity of 47.7%) are plotted alongside data from Aversa and Evangelista (1998) (FGT - fine-grained Neapolitan tuff; porosity 47%), Zhu et al. (2011) (PA - Tufo del Palatino (porosity 32%); PI - Tufo Pisolitico (porosity 35–36%), and Heap et al. (2015) (WI21 - tuff from Whakaari; porosity 28–30%) in Fig. 13. The data of Fig. 13 show that the UGT is much weaker than the other tuffs studied. Although this can be largely explained by the lower porosity of the other tuffs, we note that the UGT is also considerably weaker than the similarly-porous fine-grained Neapolitan tuff (Aversa and Evangelista, 1998). This is likely the result of the large pores (sometimes a few mm in diameter) present within the UGT (Fig. 5). By contrast, 75% of the pores within the fine-grained Neapolitan tuff had a radius < 1 μm (Aversa and Evangelista, 1998). These data (Fig. 13) therefore highlight that porosity and pore size are important in controlling the mechanical behaviour of porous tuff.

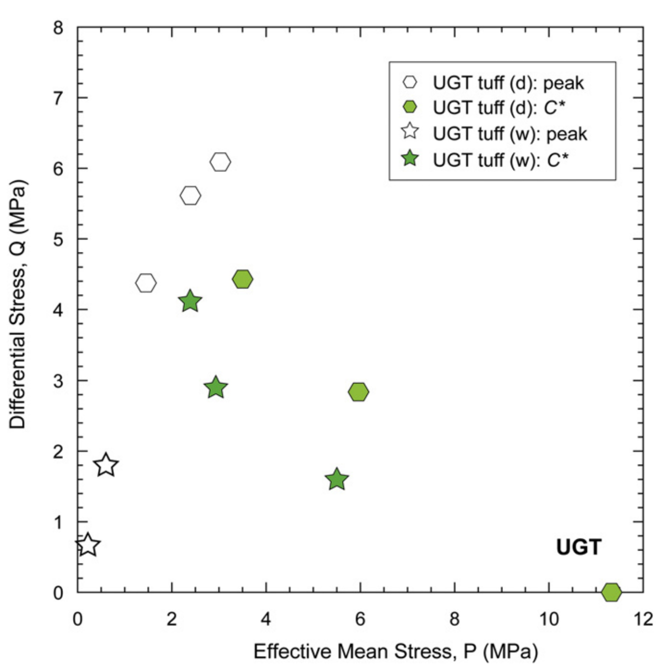

Fig. 12. Failure envelopes (in P-Q space) for UGT deformed under dry and wet conditions.

The presence of water influenced the mechanical behaviour of both tuffs under triaxial conditions. We find that the peak stress at an equivalent effective pressure is lower when wet than in the dry condition (Figs. 9 and 10), as observed in the uniaxial experiments (Fig. 11). Interestingly, we also find that the presence of water can suppress dilation (when comparing experiments performed at the same effective pressure) and may therefore be able to alter the failure mode. Although the experiments performed on dry and wet LGT at an effective pressure of 5 MPa were both dilatant (i.e. brittle) (Figs. 9b and 10b), the experiment performed in the wet condition did not dilate to the same extent as the dry experiment (Figs. 9b and 10b). We speculate the brittle-ductile transition in both tuffs is likely shifted to lower effective pressures in the presence of water. We interpret the change in mechanical behaviour due to the presence of water as the result of the presence of analcime and phillipsite (zeolites) within UGT and LGT (Altaner et al., 2013; Della Seta et al., 2015b; Fig. 5).

It has been clearly demonstrated that repeated wetting and drying cycles can control the swelling behaviour in clay rocks, irreversibly affecting its stress-strain behaviour (Vergara and Triantafyllidis, 2015). It follows that the observed strength decay might represent the minimum condition. For this reason, the impact of this effect on failure mode (i.e. suppression of dilation) could be underestimated in the experiments performed herein.

5.4. Post-deformation permeability measurements

Gas permeability measurements (performed under a confining pressure of 1 MPa) showed that the permeability of the UGT increased and decreased by a factor of two following deformation at effective pressures between 0 and 2 MPa and at 5 MPa, respectively. However, while the experiments between 0 and 0.5 MPa were dilatant, and therefore we can expect an increase in permeability due to the increase in microcrack porosity and the formation of a shear fracture (Farquharson et al., 2016), the experiments performed at effective pressures from 1 to 5 MPa were compactant (Fig. 8a). While this appears counterintuitive, because the porosity is decreasing, an increase in permeability at the initial stages of compactant (ductile) deformation has been previously observed in porous andesites (Loaiza et al., 2012; Farquharson et al., 2016). It is interpreted in these studies, and here, that distributed microcracking at the early stages of ductile deformation serves to interconnect isolated porosity thereby forming more efficient pathways for fluid flow in the samples. The permeability of the LGT increased by up to two orders of magnitude following deformation at effective pressures between 0 and 5 MPa (Fig. 10), interpreted here as the result of the formation of a shear fracture (Farquharson et al., 2016). The increase in permeability was dramatically reduced following deformation at an effective pressure of 10 MPa (Fig. 10), a consequence of the compactant nature of the LGT at this effective pressure (Fig. 8b).

5.5. Implications for slope stability at Mt. Nuovo

DSGSD are commonly constrained by geo-structural and weathering conditions; faults and joint sets, as well as meso- or micro-scale folding and foliation (Zorzi et al., 2014), provide ubiquitous anisotropy within the rock mass and/or produce weak layers where slope deformation can initiate and progress (Hou et al., 2014). Pervasive rock chemical alteration and physical degradation are often invoked, while the contribution of mechanical failure modes on slope-scale dynamics are usually less considered (Eberhardt et al., 2004). The geological setting of Mt. Nuovo (Della Seta et al., 2015a, 2015b) demonstrates that the inherited volcano-tectonic structures (i.e. NE — SW fault related to resurgence) of the slope play a crucial role in conditioning the ongoing DSGSD. In particular, the geological setting, together with the depth and geometry of

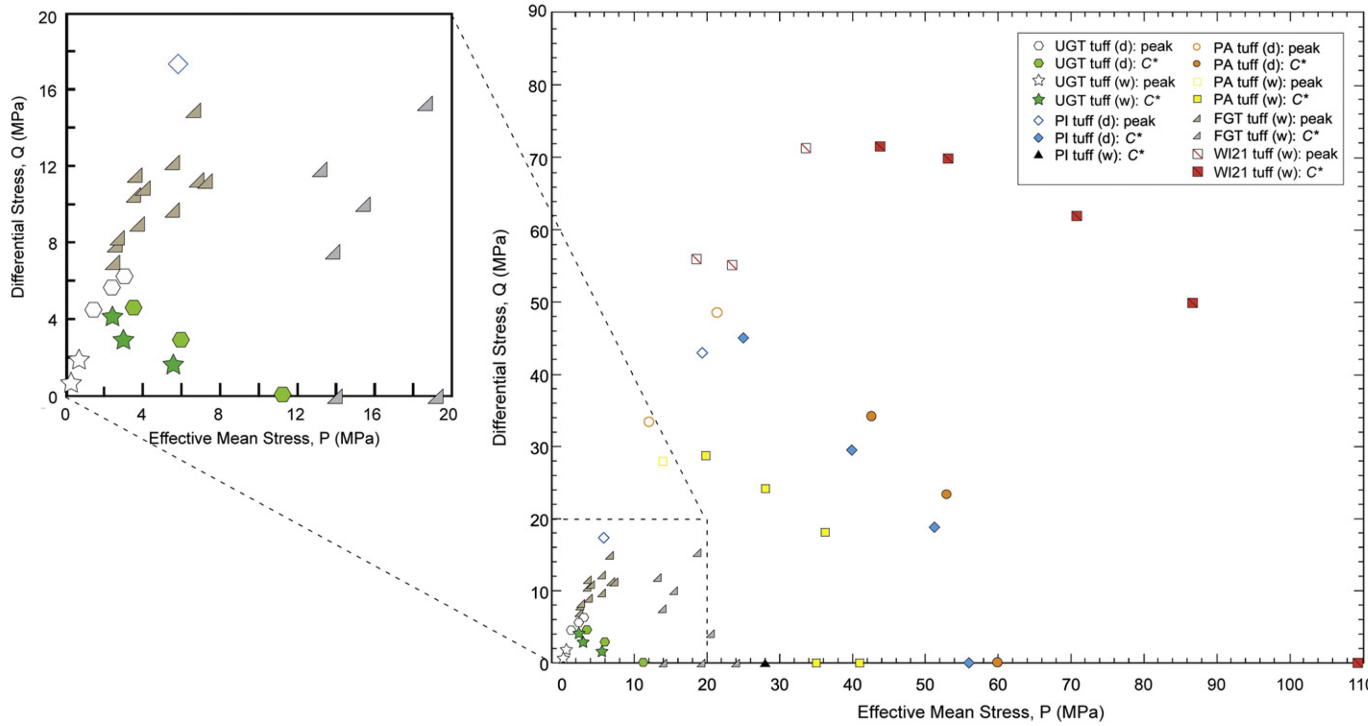

Fig. 13. Failure envelopes (in P-Q space) for UGT deformed under dry and wet conditions, plotted alongside data from Aversa and Evangelista (1998) (FGT - fine-grained Neapolitan tuff; porosity 47%), Zhu et al. (2011) (PA - Tufo del Palatino (porosity 32%); PI - Tufo Pisolitico (porosity 35–36%), and Heap et al. (2015) (WI21 - tuff from Whakaari; porosity 28–30%). Modified after Zhu et al. (2011).

shear zone, induces a structural control on the kinematic elements resulting in shear zone clustering and growth, constraining the geometry of biplanar compound slide. The high-angle tectonic elements and basal permeable lithic breccia layers have been ascribed an important role in the underground fluid circulation and outgassing (Galindo et al., 2005).

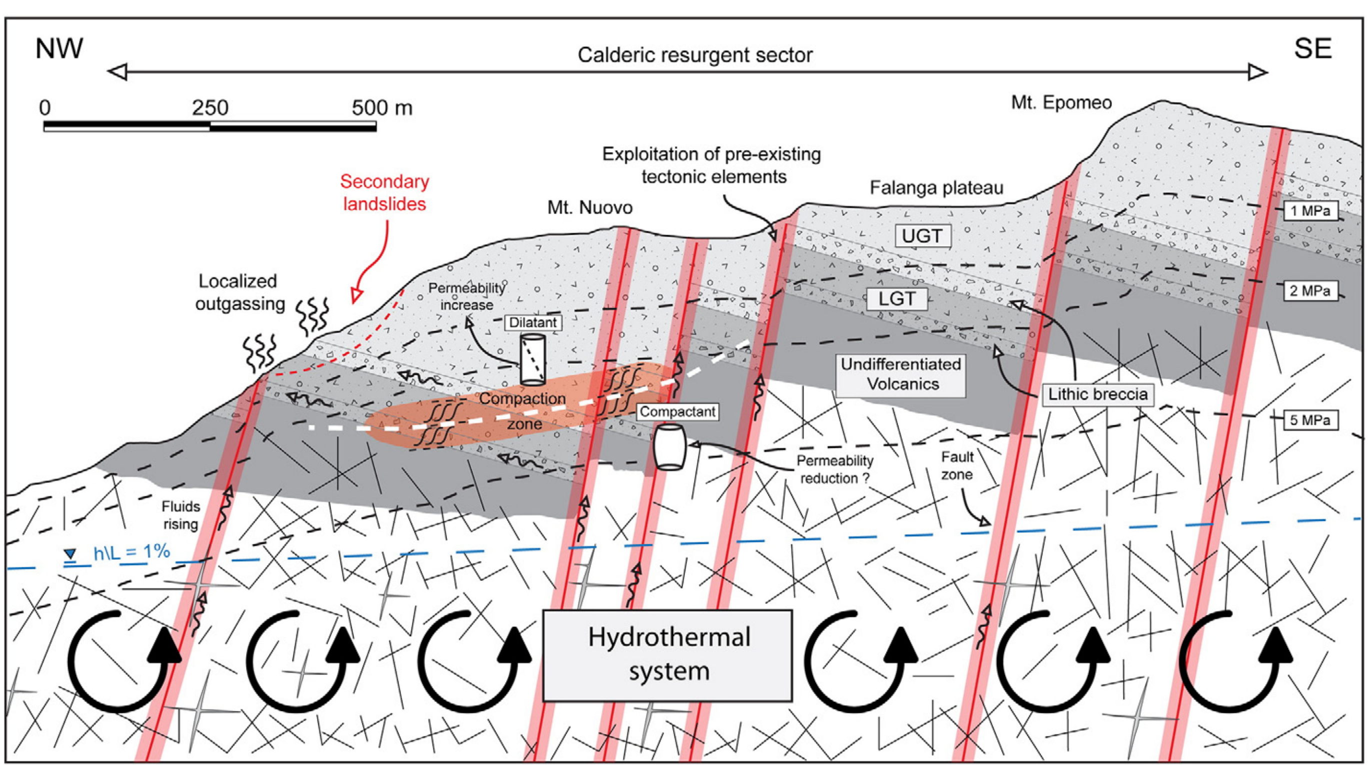

Fig. 14. Schematic cross section of the Mt. Nuovo (NW flank Mt. Epomeo) slope before the onset of deep-seated gravitational slope deformation. Fluids rise from the shallow convective hydrothermal system along tectonic elements and can move laterally within more permeable levels of lithic breccias when they reach the LGT, which is characterised by a much lower permeability. As a result, the fluids emerge on the slope face, forming a fumarolic field. The failure mode transition (brittle to ductile) occurs at a shallow level, where a compaction zone favours shear zone nucleation. Isobars of lithostatic (i.e. confining pressure) obtained by preliminary stress-strain numerical modelling are shown by the black dashed lines.

Our triaxial deformation experiments have shown that the failure mode of dry and wet UGT will transition from brittle to ductile at a depth of 100 − 200 m (i.e. depths relevant for the Mt. Nuovo slope) (Figs. 9, 10 and 14). Although the experiments on dry LGT show that compactant (ductile) behaviour occurs at a lithostatic pressure equivalent to a depth greater than the basal contact of LGT (i.e. within the underlying trachytic lavas in Mt. Nuovo; Della Seta et al., 2015b) (Fig. 8b), the presence of water may move the brittle-ductile transition to shallower depths (i.e. depths relevant for the Mt. Nuovo slope) (Fig. 9b). We also highlight that compactant (ductile) deformation requires a lower differential stress as effective pressure (i.e. depth) increases (Fig. 12). Therefore, the slope will be increasingly prone to inelastic compaction as depth increases. We further note that influxes of meteoric water and hydrothermal activity will not only weaken the UGT and LGT (since wet strength is consistently lower than dry strength; Fig. 11), but may also push the brittle-ductile transition to shallower depths. For these reasons, inelastic compaction (cataclastic pore collapse) may be the mechanism that explains the concentration of shear strains responsible for driving the DSGSD at Mt. Nuovo. Importantly, the strong influence of the presence of water on the mechanical behaviour of the tuffs highlights the importance of the hydrothermal system in governing the mechanism of the slope deformation.

Volume reduction driven by cataclastic pore collapse may have contributed to the formation of the thick shear zone where lithostatic stresses are sufficiently high to promote inelastic compaction. As noted above, ductile deformation can occur at low differential stress. Building on the theoretical approaches proposed so far (Mencl, 1968; Feda, 1973; Mahr, 1977), the combination of brittle and ductile behaviour may be responsible for the large-scale slope deformation. We propose that deformation occurs in a flow-like compactive manner upslope, where the shear zone is under a higher lithostatic pressure (Fig. 14), and in a brittle manner downslope, where the shear zone is more surficial. The discrete brittle shearing surfaces (Fig. 14) and the related dilatant MRC are reflected in the observed bulging and associated shallow landsliding at the observed at the foot of the slope (Della Seta et al., 2012). This observation is in contrast to the model described by Feda (1973) in which no bulges were found and downward failure evolution was assumed. Based on this stress-strain conceptual model, the progressive slope failure migrated upslope at Mt. Nuovo, generating a compactant shear zone that terminates on the inherited sub-vertical fault zones (Fig. 14).

The theory for mass rock deformation by compactant creep was revised by Mahr (1977) to explain the mechanisms of deep-seated gravitational slope deformation of the granodiorites of Chabenec Ridge (Mt. Tatras). The idea was originally proposed by Nemcok (1972), who considered a compactant shear zone to justify volume changes and mass balances. Although it requires very high stress to evolve (Crosta, 1996), and that most of the deep-seated gravitational slope deformation is the result of mass rock creep (Chigira, 1992), the high porosity and the very shallow brittle to ductile transition for the Mt. Nuovo tuffs (i.e. the MEGT), as well as the high temperature typical of volcanic and hydrothermal environments, could be the specific condition where compactant creep can operate efficiently. Although transient exposure to high temperature (up to 300 °C) did not greatly influence the short-term strength of the UGT and LGT, the long-term strength of tuff, at least in the brittle regime, is significantly influenced by in-situ temperatures as low as 80 °C (Ye et al., 2015). For instance, time-to-failure in a brittle creep test was reduced from 525 to 150 mins upon increasing the temperature from 40 to 80 °C (Ye et al., 2015), a result of temperature-sensitive stress corrosion cracking (Kranz et al., 1982; Meredith and Atkinson, 1985). Although no experiments exist to date, we anticipate that increasing temperature will also increase the rate of compactant creep in tuff. We also do not rule out a change in failure mode (from brittle to ductile) upon increasing the in-situ temperature, although we note that the experiments of Ye et al. (2015) show that tuff can be brittle at in-situ temperatures of 80 °C.

Landforms (e.g., multiple trenches, Cavallin et al., 1987) and the total displacement cumulated so far along the reconstructed shear zone suggest that the gravitational deformation is already accelerating towards failure (i.e. brittle creep), the rate of which is perhaps increased by the high temperature provided by the hydrothermal system (see experiments of Ye et al., 2015). This evidence is in agreement with seismic investigations consisting of ambient noise measurements (Della Seta et al., 2015a) that output a 1D resonance of the DSGSD due to the higher porosity and jointing of the rock mass with respect to the deeper substratum. Such evidence is comparable with those deduced from the mechanical transition here described, leading us to not exclude a general slope collapse as a possible final catastrophic paroxysm (Evans et al., 2006). We further note that cyclic expansion and contraction due to temperature changes as a result of hydrothermal activity can also be responsible for rock mass thermo-mechanic fatigue, a process not limited to the shallow subsurface (Bonaccorso et al., 2010; Gischig et al., 2011), and may also contribute to the incremental inelastic strain within the rock mass.

The pre-existing tectonic elements (high angle fault zones; Fig. 14), genetically related to caldera resurgence, also provide preferential paths for fluid transport. Fluids that rise towards the surface either reach the surface at the top of the fault, or move laterally into an intersected high permeability layer, such as the basal lithic breccia, and escape where the breccia layer meets the surface (Fig. 14). Indeed, clusters of fumaroles are seen where the basal lithic breccia outcrops (as mentioned above). Our experiments have shown that brittle deformation of the tuffs can significantly increase permeability, in some cases by a couple of orders of magnitude (Fig. 10). Further, we have found that, somewhat counterintuitively, compactant behaviour at the base of the deposits can also increase permeability, interpreted here as the result of connection of previously-isolated porosity. Although these findings suggest that fluid pressurisation may become increasingly unlikely as deformation progresses, an increase in permeability could increase the flow of, and/or provide additional pathways for, hydrothermal fluids that can intensely alter the host rock. For instance, pore-filling precipitation can then reduce the permeability to a value lower than the pristine (undeformed) host rock, and hydrothermal alteration can reduce the strength of the host rock (Browne, 1978; del Potro and Hürlimann, 2009; Pola et al., 2012; Frolova et al., 2014; Wyering et al., 2014; Pola et al., 2014; Heap et al., 2015; Sanchez-Alfaro et al., 2016), factors that could initiate shallow landslides within the weathered debris cover (Fig. 14).

The increase in the pore pressure within the hydrothermal system as a result of the shallow emplacement of new magma batches from depth can reduce the effective pressure acting on a rock mass, thereby encouraging brittle deformation at depths where the rock would normally deform in a ductile manner (Farquharson et al., 2016). Earthquakes or tremors related to the volcanic system, generally characterised by short-period vibrations, could produce a transitory increase in pore pressure that could be responsible for rapid changes to the effective stress field of the rock mass. On the other hand, long-period seismicity or teleseismic events could severely influence mountain slope deformation (Hungr et al., 2014) by interacting with the slope on the slope-scale as a function of the characteristic period related to the frequency content of the seismic signal (Lenti and Martino, 2013; Lenti et al., 2015). Therefore, fluid circulation within the hydrothermal system may play a key role in influencing the mechanical behaviour of the rock and therefore the stability conditions at the slope-scale (Lénat et al., 2012; Kiryukhin et al., 2012; Kiryukhin, 2016; Reid et al., 2001; Reid, 2004; Lopez and Williams, 1993). In the case of a paroxysmal collapse, the related stress release may also indirectly influence the volcanic system and initiate explosive phreatic and hydrothermal eruptions (Bozzano et al., 2013; Procter et al., 2014; Mayer et al., 2015) and/or a tsunami wave in the Gulf of Naples.

6. Conclusions

Flanks of volcanoes and resurgent calderas are often prone to slope instabilities. Their steep topography, and the often altered and weak nature of the poorly assembled volcanic materials, renders them especially hazardous in both an economic and humanitarian sense. Here we examined DSGSD at Mt. Nuovo, a process that affects the NW sector of Mt. Epomeo on Ischia Island (Italy). Although of particular interest, the slope deformation at Mt. Epomeo is complicated by the local geological setting and enhanced by the presence of an active hydrothermal system.

To increase our understanding of this DSGSD, we performed a physical and mechanical characterisation of two ignimbrite deposits - both from the MEGT - that form a significant part of the NW sector of Mt. Epomeo. Both of the collected ignimbrites are involved in the deformation of the slope. With this aim in mind, we investigated the influence of water and thermal stresses on the mechanical behaviour of MEGT tuffs. We find that the presence of water dramatically reduced the strength of the MEGT, in both the uniaxial and triaxial case, suggesting that meteoric water or the movement of fluids within the hydrothermal system could dramatically impact slope stability. Although our results show that transient exposure to 300 °C does not influence the short-term strength of the tuffs that comprise the MEGT, we highlight that the high in-situ temperature could increase the efficiency of brittle and compactant creep and therefore increase the rate of slope deformation. Our triaxial experiments show that the MEGT are capable of deforming in a compactant (ductile) manner at a depth of a couple of hundred metres (i.e. at depths relevant for the slope). We hypothesise that the compaction of the MEGT at the base of the layer could assist the onset and development of the DSGSD at Mt. Nuovo (captured in our schematic cross section; Fig. 14). Ancillary permeability measurements show that permeability increases following deformation in both the brittle and ductile regimes. Brittle deformation provides additional microcrack porosity and a shear fracture that serve to increase permeability, while ductile deformation, although compactant (i.e. porosity is reduced), increases permeability through the connection of previously-isolated porosity. An increase in permeability could promote fluid circulation and therefore alteration and pore-filling precipitation, weakening the rock and decreasing its permeability (perhaps to a value lower than that of the pristine host rock), respectively. Taken together, our experimental data highlight a potentially important role for the hydrothermal system in dictating the DSGSD at Mt. Nuovo, acting as active and passive control that conditions the short- and long-term response of the volcanic slopes. The laboratory data presented herein will be used for geomechanical zoning of an engineering-geological cross section to perform stress-strain numerical models aimed at depicting scenarios of future evolution for the DSGSD at Mt. Nuovo.

The data presented herein will help (1) evaluate the mechanical response of the slope system with respect to transient input, (2) estimate the influence of thermo-mechanical and long-term mechanisms on MRC, and (3) understand the possible evolution of the DSGSD at Mt. Nuovo towards a generalised paroxysmal failure which represents, because of its ability to trigger tsunami waves and hydrothermal or magmatic eruptions, a crucial topic in multi-risk management in the Mediterranean area.

Acknowledgements

This research was funded by “Sapienza” University of Rome under the project “Influence of geothermal systems and related thermal regime variations on the onset and development of large slope instabilities in the island of Ischia” (Year 2015 - prot. C26A15FH3L - P.I. Dr. Carlo Esposito) and by the “Partenariats Hubert Curien (PHC) GALILEE 2016-2017” grant (project number 37180VC) “Landslide-triggered tsunami hazard in the Mediterranean: improving risk mitigation strategies by understanding natural processes” (P.I. Dr. Michael Heap and Prof. Salvatore Martino). The authors are grateful to Dr. C. Perinelli and Stefano Stellino for the essential contribution to petrographic and XRPD analysis. The authors also wish to thank B. Renaudié, L. Griffiths, Prof. P. Baud, and Dr. J.I. Farquharson for their useful suggestions and support during the laboratory work. We thank Antonio Pola, one anonymous reviewer, and the editor Kelly Russell for comments that helped us improve this manuscript.

References

Acocella, V., Cifelli, F., Funiciello, R., 2001. The control of overburden thickness on resurgent domes: insights from analogue models. J. Volcanol. Geotherm. Res. 111, 137–153.

Acocella, V., Funiciello, R., 1999. The interaction between regional and local tectonics during resurgent doming: the case of the island of Ischia, Italy. J. Volcanol. Geotherm. Res. 88, 109–123.

Adelinet, M., Fortin, J., Schubnel, A., Guéguen, Y., 2013. Deformation modes in an Icelandic basalt: from brittle failure to localized deformation bands. J. Volcanol. Geotherm. Res. 255, 15–25.

Agliardi, F., Crosta, G., Zanchi, A., 2001. Structural constraints on deep seated slope deformation kinematics. Eng. Geol. 59:83–102. http://dx.doi.org/10.1016/S0013-7952(00)00066-1.

Alessio, G., Esposito, E., Ferranti, L., Mastrolorenzo, G., Porfido, S., 1996. Correlazione tra sismicità ed elementi strutturali nell'isola di Ischia. Il Quaternario. Ital. J. Quat. Sci. 9 (1), 303–308.

Al-Harthi, A.A., Al-Amri, R.M., Shehata, W.M., 1999. The porosity and engineering properties of vesicular basalt in Saudi Arabia. Eng. Geol. 54 (3), 313–320.

Alm, O., Jaktlund, L.L., Shaoquan, K., 1985. The influence of microcrack density on the elastic and fracture mechanical properties of Stripa granite. Phys. Earth Planet. Inter. 40 (3), 161–179.

Altaner, S., Demosthenous, C., Pozzuoli, A., Rolandi, G., 2013. Alteration history of Mount Epomeo Green Tuff and a related polymictic breccia, Ischia Island, Italy: evidence for debris avalanche. Bull. Volcanol. 75 (5) (doi:10.1007s00445-013-0718-1).

Ambrosi, C., Crosta, G.B., 2006. Large sackung along major tectonic features in the Central Italian Alps. Eng. Geol. 83, 183–200.

Appleton, J.D., 1972. Petrogenesis of potassium rich lavas from the Roccamonfina volcano, Roman Region, Italy. J. Petrol. 13, 425–456.

Ascione, A., Cinque, A., Franza, A., Romano, P., 2007. The geomorphic control on the initiation and propagation of the Mt. di Vezzi landslides (Ischia Island, Italy) occurred on 30th April 2006. Ital. J. Eng. Geol. Environ. 7 (2), 93–118.

Aversa, S., Evangelista, A., 1998. The mechanical behaviour of a pyroclastic rock: yield strength and “destructuration” effects. Rock Mech. Rock Eng. 31 (1), 25–42.

Bailey, R.A., Dalrymple, G.B., Lanphere, M.A., 1976. Volcanism, structure, and geochronology of Long Valley Caldera, Mono County, California. J. Geophys. Res. 81, 725–744.

Barton, N., 2002. Some new Q-value correlations to assist in site characterisation and tunnel design. Int. J. Rock Mech. Min. Sci. 39 (2), 185–216.

Baud, P., Vinciguerra, S., David, C., Cavallo, A., Walker, E., Reuschlé, T., 2009. Compaction and failure in high porosity carbonates: mechanical data and microstructural observations. Pure Appl. Geophys. 166:869–898. http://dx.doi.org/10.1007/s00024-009-0493-2.

Baud, P., Zhu, W., Wong, T.F., 2000. Failure mode and weakening effect of water on sandstone. J. Geophys. Res. 105 (B7):16,371–389. http://dx.doi.org/10.1029/2000JB900087.

Bauer, S.J., Friedman, M., Handin, J., 1981. Effects of water-saturation on strength and ductility of three igneous rocks at effective pressures to 50 MPa and temperatures to partial melting. The 22nd US Symposium on Rock Mechanics (USRMS). American Rock Mechanics Association.

Bonaccorso, A., Bonforte, A., Gambino, S., 2010. Thermal expansion-contraction and slope instability of a fumaroles field inferred from geodetic measurements at Vulcano. Bull. Volcanol. 72:791–801. http://dx.doi.org/10.1007/s00445-010-0366-7.

Bourbié, T., Zinszner, B., 1985. Hydraulic and acoustic properties as a function of porosity in Fontainebleau sandstone. J. Geophys. Res. Solid Earth 90 (B13), 11524–11532.

Bozzano, F., Gaeta, M., Lenti, L., Martino, S., Paciello, A., Palladino, D.M., Sottili, G., 2013. Modeling the effects of eruptive and seismic activities on flank instability at Mount Etna, Italy. J. Geophys. Res.: Solid Earth 118:5252–5273. http://dx.doi.org/10.1002/jgrb.50377.

Brown, R.J., Civetta, L., Arienzo, I., D'Antonio, M., Moretti, R., Orsi, G., Tomlinson, E.L., Albert, P.G., Menzies, M.A., 2014. Geochemical and isotopic insights into the assembly, evolution and disruption of a magmatic plumbing system before and after a cataclysmic caldera-collapse eruption at Ischia volcano (Italy). Contrib. Mineral. Petrol. 168:1035. http://dx.doi.org/10.1007/s00410-014-1035-1.

Brown, R.J., Orsi, G., de Vita, S., 2008. New insights into late Pleistocene explosive volcanic activity and caldera formation on Ischia (southern Italy). Bull. Volcanol. 70:583–603. http://dx.doi.org/10.1007/s00445-007-0155-0.

Browne, P.R.L., 1978. Hydrothermal alteration in active geothermal fields. Annu. Rev. Earth Planet. Sci. 6, 229–250.

Buchner, G., 1986. Eruzioni vulcaniche e fenomeni vulcano tettonici di età preistorica e storica nell'isola d'Ischia. In: Centre Jean Bérard, Institut Français de Naples (Ed.), Tremblements de terre, Eruptions Volcaniques et vie des Hommes dans la Campanie Antique. 7, pp. 145–188.

Buchner, G., Italiano, A., Vita-Finzi, C., 1996. Recent uplift of Ischia, southern Italy. Geol. Soc. London, Spec. Publ. 110:249–252. http://dx.doi.org/10.1144/GSL.SP.1996.110.01.19.

Carlino, S., Somma, R., Troiano, A., Di Giuseppe, M.G., Troise, C., De Natale, G., 2014. The geothermal system of Ischia Island (southern Italy): critical review and sustainability analysis of geothermal resource for electricity generation. Renew. Energy 62, 177–196.

Carlino, S., Somma, R., Troise, C., De Natale, G., 2012. The geothermal exploration of campanian volcanoes: historical review and future development. Renew. Sust. Energ. Rev. 16 (1) (1004e30).

Cataldi, R., Mongelli, F., Squarci, P., Taffi, L., Zito, G., Calore, C., 1991. Geothermal ranking of Italian territory. Geothermics 24, 115–129.

Cavallin, A., Crescenti, U., Dramis, F., Prestininzi, A., Sorriso-Valvo, M., 1987. Tipologia e diffusione delle deformazioni gravitative profonde di versante in Italia: prime valutazioni. Mem. Soc. Geol. Ital. 37, 241–525.

Chen, J.K., Taylor, F.W., Edwards, L.R., Cheng, H., Burr, G.S., 1995. Recent emerged reef terraces of the Yenkahe resurgent block, Tanna, Vanuatu: implications for volcanic, landslide and tsunami hazards. J. Geol. 103, 577–590.

Chiesa, S., Civetta, L., De Lucia, M., Orsi, G., Poli, S., 1987. Volcanological evolution of the island of Ischia. Rend Acc Sci Fis Mat Napoli. Special Issue, pp. 69–83.

Chigira, M., 1992. Long-term gravitational deformation of rocks by mass rock creep. Eng. Geol. 32, 157–184.

Chiocci, F.L., de Alteriis, G., 2006. The ischia debris avalanche: first clear submarine evidence in the Mediterranean of a volcanic island prehistorical collapse. Terra Nova 18, 202–209.

Chiodini, G., Avino, R., Brombach, T., Caliro, S., Cardellini, C., de Vita, S., Frondini, F., Marotta, E., Ventura, G., 2004. Fumarolic and diffuse soil degassing west of Mount Epomeo, Ischia (Italy). J. Volcanol. Geotherm. Res. 133, 291–309.

Civetta, L., Cornette, Y., Gillot, P.Y., Orsi, G., 1988. The eruptive history of Pantelleria (Sicily Channel) in the last 50 ka. Bull. Volcanol. 50, 47–57.

Civetta, L., Gallo, G., Orsi, G., 1991. Sr- and Nd-isotope and trace element constraints on the chemical evolution of the magmatic system of Ischia (Italy) in the last 55 ka. J. Volcanol. Geotherm. Res. 46, 213–230.

Clague, D.A., Denlinger, R.P., 1994. Role of olivine cumulates in destabilizing the flanks of Hawaiian volcanoes. Bull. Volcanol. 56, 425–434.

Cole, J.W., Milner, D.M., Spinks, K.D., 2005. Calderas and caldera structures: a review. Earth Sci. Rev. 69, 1–26.

Crosta, G., 1996. Landslide, spreading, deep seated gravitational deformation: analysis, examples, problems and proposal. Geogr. Fis. Din. Quat. 19, 297–313.

Crosta, G.B., Frattini, P., Agliardi, F., 2013. Deep seated gravitational slope deformations in the European Alps. Tectonophysics 605, 13–33.

Cubellis, E., 1985. Il terremoto di Casamicciola del 28 luglio 1883: analisi degli effetti, modellizzazione della sorgente ed implicazioni sulla dinamica in atto. Boll. Soc. Nat. Napoli 94, 157–186.

David, C., Menéndez, B., Darot, M., 1999. Influence of stress-induced and thermal cracking on physical properties and microstructure of La Peyratte granite. Int. J. Rock Mech. Min. Sci. 36 (4), 433–448.

Day, S.J., 1996. Hydrothermal pore fluid pressure and the stability of porous, permeable volcanoes. In: McGuire, W.J., Jones, A.P., Neuberg, J. (Eds.), Volcano Instability on the Earth and Other Planets (Geological Society Special Publication no. 110, 77 93).

de Alteriis, G., Insinga, D., Morabito, S., Morra, V., Chiocci, F.L., Terrasi, F., Lubritto, C., Di Benedetto, C., Pazzanese, M., 2010. Age of submarine debris avalanches and tephrostratigraphy offshore Ischia Island, Tyrrhenian Sea. Ital. Mar. Geol. 278, 1–18.

de Alteriis, G., Violante, C., 2009. Catastrophic landslides off Ischia volcanic island (Italy) during prehistory. Geol. Soc. Lond. Spec. Publ. 322, 73–104.

De Gennaro, M., Ferreri, M., Ghiara, M.R., Stanzione, D., 1984. Geochemistry of thermal waters on the Island of Ischia (Campania, Italy). Geothermics 13 (4), 361e74.

de Vita, S., Di Vito, M.A., Gialanella, C., Sansivero, F., 2013. The impact of the Ischia Porto Tephra eruption (Italy) on the Greek colony of Pthekoussai. Quat. Int. http://dx.doi.org/10.1016/j.quaint.2013.01.002.

de Vita, S., Sansivero, F., Orsi, G., Marotta, E., 2006. Cyclical slope instability and volcanism related to volcano-tectonism in resurgent calderas: the Ischia island (Italy) case study. Eng. Geol. 86, 148–165.

de Vita, S., Sansivero, F., Orsi, G., Marotta, E., Piochi, M., 2010. Volcanological and structural evolution of the Ischia resurgent caldera (Italy) over the past 10 ky. Geol. Soc. Am. Spec. Pap. 464, 193e241.

del Potro, R., Hürlimann, M., 2009. The decrease in the shear strength of volcanic materials with argillic hydrothermal alteration, insights from the summit region of Teide stratovolcano, Tenerife. Eng. Geol. 104, 135–143.

Del Prete, S., Mele, R., 2006. Il contributo delle informazioni storiche per la valutazione della propensione al dissesto nell'Isola d'Ischia. Rend. Soc. Geol. Ital. Nuova Serie 2, 29–47.

Della Seta, M., Esposito, C., Marmoni, G.M., Martino, S., Paciello, A., Perinelli, C., Sottili, G., 2015a. High-resolution geological model of the gravitational deformation affecting the western slope of Mt. Epomeo (Ischia). Rend. Online Soc. Geol. Ital. 35:104–108. http://dx.doi.org/10.3301/ROL.2015.75.

Della Seta, M., Esposito, C., Marmoni, G.M., Martino, S., Paciello, A., Perinelli, C., Sottili, G., 2015b. Geological constraints for a conceptual evolutionary model of the slope deformations affecting Mt. Nuovo at Ischia (Italy). Ital. J. Eng. Geol. Environ. 2:15–28. http://dx.doi.org/10.4408/IJEGE.2015-02.O-02.

Della Seta, M., Esposito, C., Marmoni, G.M., Martino, S., Scarascia Mugnozza, G., Troiani, F., 2017. Morpho-structural evolution of the valley-slope systems and related implications on slope-scale gravitational processes: new results from the Mt. Genzana case history (Central Apennines, Italy). Geomorphology 289:60–77. http://dx.doi.org/10.1016/j.geomorph.2016.07.003.

Della Seta, M., Marotta, E., Orsi, G., de Vita, S., Sansivero, F., Fredi, P., 2012. Slope instability induced by volcano-tectonics as an additional source of hazard in active volcanic areas: the case of Ischia island (Italy). Bull. Volcanol. http://dx.doi.org/10.1007/s00445-011-0501-0.

Demarco, M.M., Jahns, E., Rüdrich, J., Oyhantcabal, P., Siegesmund, S., 2007. The impact of partial water saturation on rock strength: an experimental study on sandstone [Der Einfluss einer partiellen Wassersättigung auf die mechanischen Gesteinseigenschaften: eine Fallstudie an Sandsteinen]. Z. Dtsch. Ges. Geowiss. 158 (4), 869–882.

Deriszadeh, M., Wong, R.C.K., 2014. One-dimensional swelling behaviour of clay and shale under electrical potential gradient. Transp. Porous Media 101:35–52. http://dx.doi.org/10.1007/s11242-013-0229-8.

Di Napoli, R., Aiuppa, A., Bellomo, S., Brusca, L., D'Alessandro, W., Gagliano, Candela E., Longo, M., Pecoraino, G., Valenza, M., 2009. A model for Ischia hydrothermal system: evidences from the chemistry of thermal groundwaters. J. Volcanol. Geotherm. Res. 186, 133–159.

Di Napoli, R., Federico, C., Aiuppa, A., D'Antonio, M., Valenza, M., 2013. Quantitative models of hydrothermal fluid–mineral reaction: the Ischia case. Geochim. Cosmochim. Acta 105, 108–129.

Di Napoli, R., Martorana, R., Orsi, G., Aiuppa, A., Camarda, M., Gregorio, De, Gagliano, S., Candela, E., Luzio, D., Messina, N., Pecoraino, G., Bitetto, M., de Vita, S., Valenza, M., 2011. The structure of a hydrothermal system from an integrated geochemical, geophysical, and geological approach: the Ischia Island case study. Geochem. Geophys. Geosyst. 12, 1–25.

Dramis, F., Sorriso-Valvo, M., 1994. Deep-seated gravitational slope deformations, related landslides and tectonics. Eng. Geol. 38, 231–243.

Eberhardt, E., Stead, D., Coggan, J.S., 2004. Numerical analysis of initiation and progressive failure in natural rock slopes-the 1991 Randa rockslide. Int. J. Rock Mech. Min. Sci. 41: 69–87. http://dx.doi.org/10.1016/S1365-1609(03)00076-5.

El-Naqa, A., 2001. The hydraulic conductivity of the fractures intersecting Cambrian sandstone rock masses, central Jordan. Environ. Geol. 40, 973–982.

Esposito, C., Martino, S., Scarascia Mugnozza, G., 2007. Mountain slope deformations along thrust fronts in jointed limestone: an equivalent continuum modelling approach. Geomorphology 90, 55–72.

Evans, S.G., Scarascia Mugnozza, G., Strom, A., Hermanns, R.L., 2006. Landslides From Massive Rock Slope Failure. Nato Science Series: IV. vol. 49. http://dx.doi.org/10.1007/978-1-4020-4037-5 (XVI, 662).

Farquharson, J.I., Baud, P., Heap, M.J., 2016. Inelastic compaction and permeability evolution in volcanic rock. Solid Earth Discuss. http://dx.doi.org/10.5194/se-2016-166.

Farquharson, J.I., Heap, M.J., Baud, P., 2016. Strain-induced permeability increase in volcanic rock. Geophys. Res. Lett.:43 http://dx.doi.org/10.1002/2016GL071540.

Farquharson, J.I., Heap, M.J., Baud, P., Reuschlé, T., Varley, N., 2016. Pore pressure embrittlement in a volcanic edifice. Bull. Volcanol. 78 (6). http://dx.doi.org/10.1007/s00445-015-0997-9.

Farquharson, J.I., Heap, M.J., Lavallée, Y., Varley, N., Baud, P., 2016. Evidence for the development of permeability anisotropy in lava domes and volcanic conduits. J. Volcanol. Geotherm. Res. 323, 163–185.

Feda, J., 1973. Stability of natural slopes. Proc. 8th Int. Conf. Smfe, Session 6, Oral Discussion, Moskva.

Fredrich, J.T., Wong, T.F., 1986. Micromechanics of thermally induced cracking in three crustal rocks. J. Geophys. Res. 91, 743–764.

Frolova, J., Ladygin, V., Rychagov, S., Zukhubaya, D., 2014. Effects of hydrothermal alterations on physical and mechanical properties of rocks in the Kuril–Kamchatka island arc. Eng. Geol. 183, 80–95.

Galindo, I., Soriano, C., Martí, J., Pérez, N., 2005. Graben structure in the Las Cañadas edifice (Tenerife, Canary Islands): implications for active degassing and insights on the caldera formation. J. Volcanol. Geotherm. Res. 144, 73–87.

Gischig, V.S., Moore, J.R., Evans, K.F., Amann, F., Loew, S., 2011. Thermomechanical forcing of deep rock slope deformation: 1. Conceptual study of a simplified slope. J. Geophys. Res. Earth Surf. 116 (F4).

Glicken, H., 1998. Rockslide-debris avalanche of May 18, 1980, Mount St Helens volcano, Washington. Bull. Geol. Soc. Jpn. 49, 55–106.

Gonzales, K., Finizola, A., Lénat, J., Macedo, O., Ramos, D., Thouret, J., Fournier, N., Cruz, V., Pistre, K., 2014. Asymmetrical structure, hydrothermal system and edifice stability: the case of Ubinas volcano, Peru, revealed by geophysical surveys. J. Volcanol. Geotherm. Res. 276:132–144. http://dx.doi.org/10.1016/j.jvolgeores.2014.02.020.

Gudmundsson, A., 1988. Formation of collapse calderas. Geology 16, 808–810.

Hawkins, A.B., McConnell, B.J., 1992. Sensitivity of sandstone strength and deformability to changes in moisture content. Q. J. Eng. Geol. Hydrogeol. 25 (2), 115–130.

Heap, M.J., Baud, P., Meredith, P.G., Vinciguerra, S., Reuschlé, T., 2014. The permeability and elastic moduli of tuff from Campi Flegrei, Italy: implications for ground deformation modelling. Solid Earth 5, 25–44.

Heap, M.J., Farquharson, J.I., Baud, P., Lavallée, Y., Reuschlé, T., 2015. Fracture and compaction of andesite in a volcanic edifice. Bull. Volcanol. 77:55. http://dx.doi.org/10.1007/s00445-015-0938-7.

Heap, M.J., Kennedy, B.M., 2016. Exploring the scale-dependent permeability of fractured andesite. Earth Planet. Sci. Lett. 447:139–150. http://dx.doi.org/10.1016/j.epsl.2016.05.004.

Heap, M.J., Kennedy, B.M., Farquharson, J.I., Ashworth, J., Mayer, K., Letham-Brake, M., Reuschlé, T., Gilg, H.A., Scheu, B., Lavallée, Y., Siratovich, P., Cole, J., Jolly, A.D., Baud, P., Dingwell, D.B., 2017. A multidisciplinary approach to quantify the permeability of the Whakaari/White Island volcanic hydrothermal system (Taupo Volcanic Zone, New Zealand). J. Volcanol. Geotherm. Res. 332:88–108. http://dx.doi.org/10.1016/j.jvolgeores.2016.12.004.

Heap, M.J., Kennedy, B., Perrin, N., Jacquemard, L., Baud, P., Farquharson, J.I., Scheu, B., Lavallée, Y., Gilg, H.A., Letham-Brake, M., Mayer, K., Jolly, A.D., Reuschlé, T., Dingwell, D.B., 2015. Mechanical behaviour and failure modes in the Whakaari (White Island volcano) hydrothermal system, New Zealand. J. Volcanol. Geotherm. Res. http://dx.doi.org/10.1016/j.jvolgeores.2015.02.012.

Heap, M.J., Lavallée, Y., Laumann, A., Hess, K.U., Meredith, P.G., Dingwell, D.B., 2012. How tough is tuff in the event of fire? Geology 40:311–314. http://dx.doi.org/10.1130/G32940.1.

Heap, M.J., Mollo, S., Vinciguerra, S., Lavallée, Y., Hess, K.-U., Dingwell, D.B., Baud, P., Iezzi, G., 2013. Thermal weakening of the carbonate basement under Mt. Etna volcano (Italy): implications for volcano instability. J. Volcanol. Geotherm. Res. 250, 42–60.

Heap, M.J., Russell, J.K., Kennedy, L.A., 2016. Mechanical behaviour of dacite from Mount St. Helens (USA): a link between porosity and lava dome extrusion mechanism (dome or spine)? J. Volcanol. Geotherm. Res. 328:159–177. http://dx.doi.org/10.1016/j.jvolgeores.2016.10.015.
Heap, M.J., Violay, M., Wadsworth, F.B., Vasseur, J., 2017. From rock to magma and back again: the evolution of temperature and deformation mechanism in conduit margin zones. Earth Planet. Sci. Lett. 463:92–100. http://dx.doi.org/10.1016/j.epsl.2017.01.021.
Heap, M.J., Wadsworth, F.B., 2016. Closing an open system: pore pressure changes in permeable edifice rock at high strain rates. J. Volcanol. Geotherm. Res. 315:40–50. http://dx.doi.org/10.1016/j.jvolgeores.2016.02.011.
Heard, H.C., Bonner, B.P., Duba, A.G., Schock, R.N., Stephens, D.R., 1973. High Pressure Mechanical Properties of Mt. Helen, Nevada, Tuff, Rep. UCID-16261. 37 pp. Lawrence Livermore Lab., Univ. of Calif, Livermore, Calif.
Heiken, G., Goff, F., Gardner, J.N., Baldridge, W.S., 1990. The Valles/Toledo Caldera complex, Jemez volcanic field, New Mexico. Annu. Rev. Earth Planet. Sci. 18, 27–53.
Hendrickson, R.R., 1975. Preliminary report. Tests on Cores From the Wairakei Geothermal Project. Terra Tek, Wairakei, New Zealand.
Hoek, E., Bieniawski, Z.T., 1965. Brittle fracture propagation in rock under compression. Int. J. Fract. 1, 137–155.
Hoek, E., Brown, E.T., 1980. Empirical strength criterion for rock masses. J. Geotech. Geoenviron. Eng. 106 (GT9), 1013–1035.
Hoek, E., Carranza-Torres, C.T., Corkum, B., 2002. Hoek-Brown failure criterion—2002 edition. In: Hammah, R., Bawden, W., Curran, J., Telesnicki, M. (Eds.), Proceedings of the Fifth North American Rock Mechanics Symposium (NARMS-TAC). University of Toronto Press, Toronto, pp. 267–273.
Homand-Etienne, F., Houpert, R., 1989. Thermally induced microcracking in granites: characterization and analysis. Int. J. Rock Mech. Min. Sci. Geomech. Abstr. Vol. 26 (2) (Pergamon).
Hou, Y., Chigira, M., Tsou, C.Y., 2014. Numerical study on deep-seated gravitational slope deformation in a shale-dominated dip slope due to river incision. Eng. Geol. 179: 59–75. http://dx.doi.org/10.1016/j.enggeo.2014.06.020.
Hungr, O., Evans, S.G., 2004. The occurrence and classification of massive rock slope failure. Fachzeitschrift fuer Geomechanik und Ingenieurgeologie im Bauwesen und Bergbau 22 (2), 16–23.
Hungr, O., Leroueil, S., Picarelli, L., 2014. The Varnes classification of landslide types, an update. Landslides 11:167–194. http://dx.doi.org/10.1007/s10346-013-0436-y.
Hurlimann, M., Marti, J., 2000. Mechanical relationship between landslides and caldera collapses. Geophys. Res. Lett. Vol. 27 (16), 2393–2396.
Inguaggiato, S., Pecoraino, G., D'Amore, F., 2000. Chemical and isotopic characterization of fluid manifestations of Ischia Island. J. Volcanol. Geotherm. Res. 99, 151–178.
Ippolito, F., Ortolani, F., Russo, M., 1973. Struttura marginale tirrenica dell'Appennino Campano: reinterpretazione di dati di antiche ricerche di idrocarburi. Mem. Soc. Geol. Ital. 12, 227–250.
John, D.A., Sisson, T.W., Breit, G.N., Rye, R.O., Vallance, J.W., 2008. Characteristics, extent and origin of hydrothermal alteration at Mount Rainier Volcano, Cascades Arc, USA: implications for debris-flow hazards and mineral deposits. J. Volcanol. Geotherm. Res. 175, 289–314.
Kennedy, L.A., Russell, J.K., 2012. Cataclastic production of volcanic ash at Mount Saint Helens. Phys. Chem. Earth 45, 40–49 (Parts A/B/C).
Kennedy, L.A., Russell, J.K., Nelles, E., 2009. Origins of Mount St. Helens cataclasites: experimental insights. Am. Mineral. 94 (7), 995–1004.
Kiryukhin, A., 2016. Modeling and observations of geyser activity in relation to catastrophic landslides–mudflows (Kronotsky nature reserve, Kamchatka, Russia). J. Volcanol. Geotherm. Res. 323, 129–147.
Kiryukhin, A., Rychkova, T.V., Dubrovskaya, I.K., 2012. Hydrothermal system in Geysers Valley (Kamchatka) and triggers of the Giant landslide. Appl. Geochem. J. 27, 1753–1766.
Kranz, R.L., Harris, W.J., Carter, N.L., 1982. Static fatigue of granite at 200 °C. Geophys. Res. Lett. 9 (1), 1e4.
Lénat, J.-F., Bachèlery, P., Peltier, A., 2012. The interplay between collapse structures, hydrothermal systems, and magma intrusions: the case of the central area of Piton de la Fournaise volcano. Bull. Volcanol. 74 (2012):407–421. http://dx.doi.org/10.1007/s00445-011-0535-3.
Lenti, L., Martino, S., 2013. A parametric numerical study of the interaction between seismic waves and landslides for the evaluation of the susceptibility to seismically induced displacements. Bull. Seismol. Soc. Am. 103 (1), 33–56.
Lenti, L., Martino, S., Paciello, A., Prestininzi, A., Rivellino, S., 2015. Recorded displacements in a landslide slope due to regional and teleseismic earthquakes. Geophys. J. Int. 201: 1335–1345. http://dx.doi.org/10.1093/gji/ggv063.
Lima, A., Cicchella, D., Di Francia, S., 2003. Natural contribution of harmful elements in thermal groundwaters of Ischia Island (southern Italy). Environ. Geol. 43, 930–940.
Lipman, P.W., 1984. The roots of ash calderas in Western North America: windows into the tops of granitic batholits. J. Geophys. Res. 89, 8801–8841.
Lipman, P.W., 1997. Subsidence of ash-flow calderas: relation to caldera size and magma-chamber geometry. Bull. Volcanol. 59, 198–218.
Loaiza, S., Fortin, J., Schubnel, A., Guéguen, Y., Vinciguerra, S., Moreira, M., 2012. Mechanical behavior and localized failure modes in a porous basalt from the Azores. Geophys. Res. Lett.:39 http://dx.doi.org/10.1029/2012GL053218.
Lopez, D.L., Williams, N.S., 1993. Catastrophic Volcanic Collapse: Relation to Hydrothermal Processes. Science 20, 1974–1976.
Mahr, T., 1977. Deep-reaching gravitational deformations of high mountain slopes. Bull. Int. Assoc. Eng. Geol. 16:121–127. http://dx.doi.org/10.1007/BF02591467.
Manzo, M., Ricciardi, G.P., Casu, F., Ventura, G., Zeni, G., Borgström, S., Berardino, P., Del Gaudio, C., Lanari, R., 2006. Surface deformation analysis in the Ischia Island (Italy) based on spaceborne radar interferometry. J. Volcanol. Geotherm. Res. 151, 399–416.
Marmoni, G.M., Martino, S., Heap, M.J., Reuschlé, T., 2017. Multiphysics laboratory tests for modeelling gravity-driven instabilities at slope scale. Proc. Eng. 191:142–149. http://dx.doi.org/10.1016/j.proeng.2017.05.165.
Marsh, B.D., 1984. On the mechanics of caldera resurgence. J. Geophys. Res. 89, 8245–8251.
Matsuki, K., Chida, Y., Sakaguchi, K., Glover, P.W.J., 2006. Size effect on aperture and permeability of a fracture as estimated in large synthetic fractures. Int. J. Rock Mech. Min. Sci. 43, 726–755.
Mayer, K., Scheu, B., Gilg, H.A., Heap, M.J., Kennedy, B.M., Lavallée, Y., Letham-Brake, M., Dingwell, D.B., 2015. Experimental constraints on phreatic eruption processes at Whakaari (White Island volcano). J. Volcanol. Geotherm. Res. 302, 150–162.
Mazzarella, A., De, Luise E., 2007. The meteoric event of 30th April 2006 at Ischia Island, Italy. Ital. J. Eng. Geol. Environ. 7 (2), 7–14.
Mele, R., Del Prete, S., 1998. Fenomeni di instabilità dei versanti in Tufo Verde del Monte Epomeo (Isola d'Ischia—Campania). Boll. Soc. Geol. Ital. 117, 93–112.
Mencl, V., 1968. Plastizitatslehre und das wirkliche Verhalten von Gebirgsmassen. Felsmech. U. Ing. Geol. (Suppl IV), 1–8.
Meredith, P.G., Atkinson, B.K., 1985. Fracture toughness and subcritical crack growth during high-temperature tensile deformation of Westerly granite and Black gabbro. Phys. Earth Planet. In. 39 (1), 33–51.
Molin, P., Acocella, V., Funiciello, R., 2003. Structural, seis-mic and hydrothermal features at the border of an active in-termittent resurgent block: Ischia Island (Italy). J. Volcanol. Geotherm. Res. 121, 65–81.
Molina, F., Martí, J., 2016. The Borinquen geothermal system (Ca˜nas Dulces caldera, Costa Rica). Geothermics 64, 410–425.
Mollo, S., Vinciguerra, S., Iezzi, G., Iarocci, A., Scarlato, P., Heap, M.J., Dingwell, D.B., 2011. Volcanic edifice weakening via devolatilization reactions. Geophys. J. Int. 186 (3), 1073–1077.
Montanaro, C., Scheu, B., Mayer, K., Orsi, G., Moretti, R., Isaia, R., Dingwell, D.B., 2016. Experimental investigations on the explosivity of steam-driven eruptions: a case study of Solfatara volcano (Campi Flegrei). J. Geophys. Res. Solid Earth 121:7996–8014. http://dx.doi.org/10.1002/2016JB013273.
Moran-Zenteno, D.J., Alba-Aldave, L.A., Sole, J., Iriondo, A., 2004. A major resurgent caldera in southern Mexico: the source of the late Eocene Tilzapotla ignimbrite. J. Volcanol. Geotherm. Res. 136, 97–119.
Moro, M., Saroli, M., Salvi, S., Stramondo, S., Doumaz, F., 2007. The relationship between seismic deformation and deep-seated gravitational movements during the 1997 Umbria–Marche (Central Italy) earthquakes. Geomorphology 89, 297–307.
Nara, Y., Meredith, P.G., Yoneda, T., Kaneko, K., 2011. Influence of macrofractures and micro-fractures on permeability and elastic wave velocities in basalt at elevated pressure. Tectonophysics 503, 52–59.
Nemcok, A., 1972. Gravitational slope deformation in high mountains. Proc. 24th Int. Geol. Cong., Montréal, Sect. 13, pp. 132–141.
Orsi, G., de Vita, S., di Vito, M., 1996. The restless, resurgent Campi Flegrei nested caldera (Italy): constraints on its evolution and configuration. J. Volcanol. Geotherm. Res. 74, 179–214.
Orsi, G., de Vita, S., Di Vito, M., Isaia, R., Nave, R., Heiken, G., 2003. Facing volcanic and related hazards in the Neapolitan area. In: Heiken, G., Fakundiny, R., Sutter, J. (Eds.), Earth Sciences in the City. American Geophysical Union (Special Publication), Washington, pp. 121–170.
Orsi, G., Gallo, G., Zanchi, A., 1991. Simple-shearing block resurgence in caldera depression. A model from Pantelleria and Ischia. J. Volcanol. Geotherm. Res. 47, 1–11.
Orsi, G., Piochi, M., Campajola, L., D'Onofrio, A., Gialanella, L., Terrasi, F., 1996. 14C geochronological constraints for the volcanic history of the island of Ischia (Italy) over the last 5000 years. J. Volcanol. Geotherm. Res. 71, 249–257.
Paoletti, V., Langella, G., Di Napoli, R., Amoresano, A., Meo, S., Pecoraino, G., Aiuppa, A., 2015. A tool for evaluating geothermal power exploitability and its application to Ischia, Southern Italy. Appl. Energy 139, 303–312.
Paparo, M.A., Tinti, S., 2017. Analysis of seismic-driven instability of Mt. Nuovo in the Ischia Island, Italy. Bull. Seismol. Soc. Am. 107 (2). http://dx.doi.org/10.1785/0120160139.
Penta, F., Conforto, B., 1951a. Sulle misure di temperatura del sottosuolo nei fori trivellati in presenza di acqua e sui relativi rilievi freatimetrici in regioni idrotermali. Ann. Geophys. 4, 41–93.
Penta, F., Conforto, B., 1951b. Risultati di sondaggi e di ricerche geominerarie nell'Isola di Ischia dal 1939 al 1943, nel campo del vapore, delle acque termali e delle "forze endogene" in generale. Ann. Geophys. 4, 159–191.
Pola, A., Crosta, G., Fusi, N., Barberini, V., Norini, G., 2012. Influence of alteration on physical properties of volcanic rocks. Tectonophysics 566–567, 67–86.
Pola, A., Crosta, G.B., Fusi, N., Castellanza, R., 2014. General characterization of the mechanical behaviour of different volcanic rocks with respect to alteration. Eng. Geol. 169, 1–13.
Procter, J.N., Cronin, S.J., Zernack, A.V., Lube, G., Stewart, R.B., Nemeth, K., Keys, H., 2014. Debris flow evolution and the activation of an explosive hydrothermal system; Te Maari, Tongariro, New Zealand. J. Volcanol. Geotherm. Res. 286, 303–316.
Radbruch-Hall, D.H., 1978. Gravitational creep of rock masses on slopes. In: Voight, B. (Ed.), Rockslides and Avalanches. Develop. Geotec. Eng. Vol. 14. Elsevier, Amsterdam, pp. 607–658.
Reid, M.E., 2004. Massive collapse of volcano edifices triggered by hydrothermal pressurization. Geology 32:373–376. http://dx.doi.org/10.1130/G20300.1.
Reid, M.E., Sisson, T.W., Brien, D.L., 2001. Volcano collapse promoted by hydrothermal alteration and edifice shape, Mount Rainier, Washington. Geology 29, 779–782.
Reuschlé, T., Haore, S.G., Darot, M., 2006. The effect of heating on the microstructural evolution of La Peyratte granite deduced from acoustic velocity measurements. Earth Planet. Sci. Lett. 243 (3), 692–700.
Rittmann, A., 1930. Geologie der Insel Ischia. Z f Vulkanol Er-ganzungsband 6.
Romagnoli, C., Casalbore, D., Chiocci, F.L., Bosman, A., 2009. Offshore evidence of large-scale lateral collapses on the east-ern flank of Stromboli, Italy, due to structurally-controlled, bilateral flank instability. Mar. Geol. 262, 1–13.

Sanchez-Alfaro, P., Reich, M., Arancibia, G., Pérez-Flores, P., Cembrano, J., Driesner, T., Lizama, M., Rowland, J., Morata, D., Heinrich, C.A., Tardani, D., Campos, E., 2016. Physical, chemical and mineralogical evolution of the Tolhuaca geothermal system, southern Andes, Chile: insights into the interplay between hydrothermal alteration and brittle deformation. J. Volcanol. Geotherm. Res. 324, 88–104.
Sbrana, A., Fulignati, P., Marianelli, P., Boyce, A.J., Cecchetti, A., 2009. Exhumation of an active magmatic-hydrothermal system in a resurgent caldera environment: the example of Ischia (Italy). J. Geol. Soc. Lond. 166:1061–1073. http://dx.doi.org/10.1144/0016-76492009-030.
Sbrana, A., Toccaceli, R.M., 2011. Carta Geologica della regione Campania - Foglio 464, Isola di Ischia. Litografia artistica cartografica, Firenze.
Schaefer, L.N., Kendrick, J.E., Oommen, T., Lavallée, Y., Chigna, G., 2015. Geomechanical rock properties of a basaltic volcano. Front. Earth Sci. 3, 29.
Schultz, R.A., Li, Q., 1995. Uniaxial strength testing of non welded Calico Hills tuff, Yucca Mountain, Nevada. Eng. Geol. 40:287–299. http://dx.doi.org/10.1016/0013-7952(95)00041-0.
Sepe, V., Atzori, S., Ventura, G., 2007. Subsidence due to crack closure and depressurization of hydrothermal systems: a case study from Mt. Epomeo (Ischia Island, Italy). Terra Nova http://dx.doi.org/10.1111/j.1365-3121.2006.00727.x.
Shimada, M., 1986. Mechanism of deformation in a dry porous basalt at high pressures. Tectonophysics 121 (2–4), 153–173.
Siebert, L., 1984. Large volcanic debris avalanches: characteristics of source areas, deposits, and associated eruptions. J. Volcanol. Geotherm. Res. 22, 163–197.
Siratovich, P.A., Heap, M.J., Villeneuve, M.C., Cole, J., Kennedy, B.M., Davidson, J., Reuschlé, T., 2016. Mechanical behaviour of the Rotokawa Andesites (New Zealand): Insight into permeability evolution and stress-induced behaviour in an actively utilised geothermal. Geothermics 64:163–179. http://dx.doi.org/10.1016/j.geothermics.2016.05.005.
Sitharam, T.G., Sridevi, J., Shimizu, N., 2001. Practical equivalent continuum characterization of jointed rock masses. Int. J. Rock Mech. Min. Sci. 38, 437–448.
Smith, R.L., Bailey, R.A., 1968. Resurgent cauldrons. In: Coats, R.R., Hay, R.L., Anderson, C.A. (Eds.), Studies in Volcanology. Geological Society of America, Memoirs. 116, pp. 613–662.
Smith, R., Sammonds, P.R., Kilburn, C.R., 2009. Fracturing of volcanic systems: experimental insights into pre-eruptive conditions. Earth Planet. Sci. Lett. 280 (1), 211–219.
Smith, R., Sammonds, P.R., Tuffen, H., Meredith, P.G., 2011. Evolution of the mechanics of the 2004–2008 Mt. St. Helens lava dome with time and temperature. Earth Planet. Sci. Lett. 307 (1), 191–200.
Spinks, K.D., Acocella, V., Cole, J.W., Bassett, K.N., 2005. Structural control of volcanism and caldera development in the transtensional Taupo volcanic zone, New Zealand. J. Volcanol. Geotherm. Res. 144, 7–22.
Stelling, P., Shevenell, L., Hinz, N., Coolbaugh, M., Melosh, G., Cumming, W., 2016. Geothermal systems in volcanic arcs: volcanic characteristics and surface manifestations as indicators of geothermal potential and favorability worldwide. J. Volcanol. Geotherm. Res. 324:57–72. http://dx.doi.org/10.1016/j.jvolgeores.2016.05.018.
Tedesco, D., 1996. Chemical and isotopic investigations of fumarolic gases from Ischia island southern Italy: evidences of magmatic and crustal contribution. J. Volcanol. Geotherm. Res. 74, 233–242.
Tibaldi, A., Vezzoli, L., 1998. The space problem of caldera resurgence: an example from Ischia Island, Italy. Geol. Rundsch. 87, 53–66.
Tinti, S., Chiocci, F.L., Zaniboni, F., Pagnoni, G., de Alteriis, G., 2011. Numerical simulation of the tsunami generated by a past catastrophic landslide on the volcanic island of Ischia, Italy. Mar. Geophys. Res. 32 (1):287–297. http://dx.doi.org/10.1007/s11001-010-9109-6.
Tomlinson, E.L., Albert, P.G., Wulf, S., Brown, R.J., Smith, V.C., Keller, J., Orsi, G., Bourne, A.J., Menzies, M.A., 2014. Age and geochemistry of tephra layers from Ischia, Italy: constraints from proximal-distal correlations with Lago Grande di Monticchio. J. Volcanol. Geotherm. Res. 287, 22–39.
Topal, T., Doyuran, V., 1997. Engineering geological properties and durability assessment of the Cappadocian tuff. Eng. Geol. 47:175–187. http://dx.doi.org/10.1016/S0013-7952(97)00017-3.
Topal, T., Sözmen, B., 2003. Deterioration mechanisms of tuffs in Midas monument. Eng. Geol. 68:201–223. http://dx.doi.org/10.1016/S0013-7952 (02)00228-4.
Tuncay, E., 2009. Rock rupture phenomenon and pillar failure in tuffs in the Cappadocia region (Turkey). Int. J. Rock Mech. Min. Sci. 46:1253–1266. http://dx.doi.org/10.1016/j.ijrmms.2009.01.011.
Ulusoy, I., Cubukcu, E., Aydar, E., Labazuy, P., Gourgaud, A., Vincent, P.M., 2004. Volcanic and deformation history of the Bodrum resurgent caldera system (southwestern Turkey). J. Volcanol. Geotherm. Res. 136, 71–96.
van Wyk de Vries, B., Kerle, N., Petley, D., 2000. Sector collapse forming at Casita volcano, Nicaragua. Geology 28 (2), 167–170.
Vásárhelyi, B., Ván, P., 2006. Influence of water content on the strength of rock. Eng. Geol. 84 (1), 70–74.
Vergara, M.R., Triantafyllidis, T., 2015. Swelling behaviour of volcanic rocks under cyclic wetting and drying. Int. J. Rock Mech. Min. Sci. 80, 231–240.
Vezzoli, L., 1988. Island of Ischia. In: Vezzoli, L. (Ed.), CNR Quaderni de "La ricerca scientifica" (114-10, 122).
Vinciguerra, S., Del Gaudio, P., Mariucci, M.T., Marra, F., Meredith, P.G., Montone, P., Scarlato, P., 2009. Physical properties of tuffs from a scientific borehole at Alban hills volcanic district (central Italy). Tectonophysics 471 (1), 161–169.
Vinciguerra, S., Trovato, C., Meredith, P.G., Benson, P.M., 2005. Relating seismic velocities, thermal cracking and permeability in Mt. Etna and Iceland basalts. Int. J. Rock Mech. Min. Sci. 42, 900–910.
Violay, M., Gibert, B., Mainprice, D., Burg, J.P., 2015. Brittle versus ductile deformation as the main control of the deep fluid circulation in oceanic crust. Geophys. Res. Lett. 42 (8), 2767–2773.
Violay, M., Gibert, B., Mainprice, D., Evans, B., Dautria, J.M., Azais, P., Pezard, P., 2012. An experimental study of the brittle-ductile transition of basalt at oceanic crust pressure and temperature conditions. J. Geophys. Res. Solid Earth 117 (B3).
Voight, B., Elsworth, D., 1997. Failure of volcano slopes. Geotechnique 47, 1–31.
Wohletz, K., Heiken, G., 1992. Volcanology and Geothermal Energy. University of California Press, Berkeley http://ark.cdlib.org/ark:/13030/ft6v19p151/.
Wong, T.F., Baud, P., 2012. The brittle-ductile transition in rocks: a review. J. Struct. Geol. 44, 25–53.
Wulf, S., Kraml, M., Brauer, A., Keller, J., Negendank, J.F.W., 2004. Tephrochronology of the 100 ka lacustrine sediment record of Lago Grande di Monticchio (southern Italy). Quat. Int. 122, 7–30.
Wyering, L.D., Villeneuve, M.C., Wallis, I.C., Siratovich, P.A., Kennedy, B.M., Gravley, D.M., Cant, J.L., 2014. Mechanical and physical properties of hydrothermally altered rocks, Taupo Volcanic Zone, New Zealand. J. Volcanol. Geotherm. Res. 288, 76–93.
Ye, G.-l, Nishimura, T., Zhang, F., 2015. Experimental study on shear and creep behaviour of green tuff at high temperatures. Int. J. Rock Mech. Min. Sci. 79, 19–28.
Zaniboni, F., Pagnoni, G., Tinti, S., Della Seta, M., Fredi, P., Marotta, E., Orsi, G., 2013. The potential failure of Monte Nuovo at Ischia Island (southern Italy): numerical assessment of a likely induced tsunami and its effects on a densely inhabited area. Bull. Volcanol. 75:763. http://dx.doi.org/10.1007/s00445-013-0763-9.
Zhu, W., Baud, P., Vinciguerra, S., Wong, T.F., 2011. Micromechanics of brittle faulting and cataclastic flow in Alban Hills tuff. J. Geophys. Res. 116B06209. http://dx.doi.org/10.1029/2010JB008046.
Zorzi, L., Massironi, M., Surian, N., Genevois, R., Floris, M., 2014. How multiple foliations may control large gravitational phenomena: a case study from the Cismon Valley, Eastern Alps, Italy. Geomorphology 207:149–160. http://dx.doi.org/10.1016/j.geomorph.2013.11.001.